JAERI-Research

JP0350571

2003-021

# EVALUATIONS OF MEDIUM-HEAVY NUCLIDE DATA FOR JENDL-3.3

September 2003

Keiichi SHIBATA, Tetsuo ASAMI*, Takashi WATANABE*
Yukinobu WATANABE*, Nobuhiro YAMAMURO*
Masayuki IGASHIRA* and Hideo KITAZAWA*

日本原子力研究所
Japan Atomic Energy Research Institute

本レポートは，日本原子力研究所が不定期に公刊している研究報告書です。
入手の問合わせは，日本原子力研究所研究情報部研究情報課（〒319－1195 茨城県那珂郡東海村）あて，お申し越しください。なお，このほかに財団法人原子力弘済会資料センター（〒319－1195　茨城県那珂郡東海村日本原子力研究所内）で複写による実費頒布をおこなっております。

This report is issued irregularly.
Inquiries about availability of the reports should be addressed to Research Information Division, Department of Intellectual Resources, Japan Atomic Energy Research Institute, Tokai-mura, Naka-gun, Ibaraki-ken 〒319－1195, Japan.



編集兼発行　日本原子力研究所

# Evaluations of Medium-heavy Nuclide Data for JENDL-3.3

Keiichi SHIBATA, Tetsuo ASAMI[*1], Takashi WATANABE[*2],
Yukinobu WATANABE[*3], Nobuhiro YAMAMURO[*4],
Masayuki IGASHIRA[*4] and Hideo KITAZAWA[*5]

Department of Nuclear Energy System
Tokai Research Establishment
Japan Atomic Energy Research Institute
Tokai-mura, Naka-gun, Ibaraki-ken

(Received August 1, 2003)

Evaluations of neutron nuclear data for medium-heavy nuclides were performed for JENDL-3.3. The present work was undertaken to remove the drawbacks of the previous library JENDL-3.2. Recent measurements and nuclear model calculations were taken into account to improve the accuracy of the evaluated data. The data on natural elements were not produced in order to solve a problem of the inconsistency between elemental and isotopic data except for carbon and vanadium in JENDL-3.3.

Keywords: JENDL-3.3, Evaluation, Neutron Nuclear Data, Cross Section, Spectrum

*1 Data Engineering, Inc.
*2 Enetec Co., Ltd.
*3 Kyushu University
*4 Tokyo Institute of Technology
*5 National Defense Academy

# JENDL-3.3 のための中重核データの評価

日本原子力研究所東海研究所エネルギーシステム研究部
柴田　恵一・浅見　哲夫[*1]・渡部　隆[*2]・渡辺　幸信[*3]
山室　信弘[*4]・井頭　政之[*4]・北沢　日出男[*5]

(2003 年 8 月 1 日受理)

JENDL-3.3 のために中重核領域の中性子核データ評価を行った。この仕事は、前版 JENDL-3.2 の欠点を解消するために行われた。最新の測定値及び理論計算値を考慮して、評価済データの精度向上に努めた。同位体データとの不一致を解消するために、JENDL-3.3 では炭素、バナジウム以外天然元素データは作成しなかった。

東海研究所：〒319-1195　茨城県那珂郡東海村白方白根 2-4
*1　(株) データ工学
*2　(株) エネテック
*3　九州大学
*4　東京工業大学
*5　防衛大学校

Contents



目 次

This is a blank page.

## 1. Introduction

The second revision of JENDL-3 (JENDL-3.2)[1] was released in 1994. Since then, the data have been used in various application fields. However, some drawbacks of the library were pointed out by comparing the data with differential and integral measurements. A task force was set up in the Japanese Nuclear Data Committee (JNDC) to examine the quality of JENDL-3.2, and the problems of the library were reported. Considering the report, evaluation work started in 1997 in cooperation with JNDC.

The Medium-heavy Nuclide Data Evaluation Working Group took the responsibility of medium-heavy nuclide data for JENDL-3.3[2]. As for medium-heavy nuclei, JENDL-3.2 has the following problems:

(1) There is inconsistency between elemental and isotopic evaluations.
(2) In the MeV region, radiative capture cross sections of many nuclei decrease rapidly with incident energy, which is unlikely to occur.
(3) Interpolation of energy distributions is inadequate especially near the threshold energy.
(4) The calculated gamma-ray heating rate for iron is much larger[3] than the data measured at the JAERI FNS facility.
(5) Angle-dependent neutron emission spectra are required for fusion neutronics calculations.
(6) Covariances are needed for some nuclei.

The problems in the items (4) and (5) had been already solved by the evaluation for JENDL Fusion File 99 (JENDL/F-99)[4], and the revised data were reflected on JENDL-3.3. Concerning the item (3), the interpolation type and the distribution at the threshold energy were changed for JENDL-3.3. We gave up making natural-element files except for carbon and vanadium in order to solve the problem given in the item (1).

Unlike heavy-nuclide data, the medium-heavy nuclide data in JENDL-3.2 have an intrinsic problem which is not common to other nuclei. Therefore, each evaluator had to look into data carefully and had to adopt various evaluation methods which are most suitable for each nuclide. This report describes the medium-heavy nuclide data ranging from $^{27}$Al to $^{209}$Bi which were revised for JENDL-3.3.

## 2. Aluminum-27

The JENDL-3.2 calculations could not reproduce the measured neutron emission spectra[5] at 18 MeV. The direct-reaction cross sections for the inelastic scattering were calculated by using the DWUCK code[6] in order to improve the quality of the evaluated data. The optical-model potential parameters are the same as those used in the evaluation for JENDL-3.2:

$V = 51.87 - 0.31E$ (MeV), $W_s = 7.14$ (MeV) if $E \geq 11$ MeV,
$V = 48.6$ (MeV), $W_s = 4.94+0.20E$ (MeV) if $E \leq 11$ MeV,
$V_{so} = 6.0$ (MeV),
$r_0 = 1.18$ (fm), $r_s = 1.26$ (fm), $r_{so} = 1.01$ (fm),
$a_0 = 0.64$ (fm), $a_s = 0.58$ (fm), $a_{so} = 0.50$ (fm).

A deformation parameter, $\beta_4 = 0.256$, was taken from the compilation[7] by Möller for $^{28}$Si. The cross sections were calculated with a weak-coupling model and added to the compound ones for the following discrete levels:

| $E_x$ (MeV) | Spin-parity | MT |
|---|---|---|
| 4.5103 | 11/2+ | 61 |
| 4.5800 | 7/2+ | 62 |
| 4.8120 | 5/2+ | 63 |
| 5.4330 | 9/2+ | 67 |
| 5.5507 | 3/2+ | 70 |

Figures 1 and 2 show comparisons of the calculated neutron emission spectra with the data measured by Baba et al.[5] at 14 MeV and 18 MeV, respectively. At 18 MeV, the present calculations still underestimate the measured spectra corresponding to the excitation energies 4-5 MeV, as seen in Fig.2. This fact should be re-considered in the future library.

The (n,2n) reaction cross section was replaced with the calculations performed by Yamamuro using the EGNASH code[8]. It is found from Fig. 3 that the revised cross sections are much lower than the JENDL-3.2 values above 15 MeV.

Double-differential neutron, proton and α-particle spectra were taken from JENDL/F-99[4].

## 3. Silicon-28

In the JENDL-3.2 evaluation, the direct-reaction cross section was not considered for the inelastic scattering to the $6^+$-state (8.5430 MeV). In the present

work, this state was regarded as a member of the ground-state rotational band of $^{28}$Si, and a coupled-channel calculation was performed by using the ECIS code[9]. Only the cross section for the $6^+$-state was revised by incorporating the coupled-channel calculations.

Double-differential neutron, proton and α-particle spectra were taken from JENDL/F-99[4].

## 4. Titanium Isotopes

The data of Ti isotopes were partly re-evaluated for JENDL-3.3. In the re-evaluation work, the JENDL-3.2 data were examined by comparing them with new experimental data and the unsatisfactory data were updated. The data on gamma production for all isotopes and the covariances for $^{48}$Ti were newly evaluated. In the compilation of JENDL-3.3, the elemental data were not produced and only the isotopic data were given. The abundance of each isotope is tabulated below:

| Isotope | Abundance (%) |
|---|---|
| $^{46}$Ti | 8.25 |
| $^{47}$Ti | 7.44 |
| $^{48}$Ti | 73.72 |
| $^{49}$Ti | 5.41 |
| $^{50}$Ti | 5.18 |

### 4.1 Resolved Resonance Parameters

The total cross sections reconstructed from the resonance parameters in JENDL-3.2 were examined by comparing them with experimental data, and some parameters for all isotopes but $^{47}$Ti were modified so as to give a better fit to the experimental data. As a result, the upper energy-limit of the resonance region was expanded except for $^{47}$Ti: 100 keV to 300 keV for $^{46}$Ti, 100 keV to 300 keV for $^{48}$Ti, 100 keV to 180 keV for $^{49}$Ti, 100 keV to 300 keV for $^{50}$Ti. The parameters for $^{47}$Ti remain unchanged from JENDL-3.2. The multi-level Breit-Wigner formula is used for each isotope to represent resonant cross sections.

### 4.2 Total, Elastic Scattering and Capture Cross Sections above the Resonance Region

In the energies above the resonance region, the total cross sections of $^{46,47,49,50}$Ti were taken from those in JENDL-3.2 which were obtained from optical-model calculations. The total cross section of $^{48}$Ti was determined by subtracting the other isotopic contributions from measured total cross sections of the element.

The pre-equilibrium component of the capture cross sections was calculated by

using the GNASH code[10], and it was added to the capture cross section in JENDL-3.2. Figure 4 illustrates the evaluated capture cross sections of elemental Ti together with experimental data. Figure 5 shows the capture cross section of $^{50}$Ti.

The elastic scattering cross sections were obtained by subtracting a sum of the partial non-elastic cross sections from the total cross sections.

### 4.3 Reaction Cross Sections

The cross-section data on some threshold reactions were revised by the statistical-model calculations using the EGNASH code[8]. Some data were taken from the JENDL special purpose libraries, JENDL Activation Cross Section File 96 (JENDL/A-96)[11] and JENDL Dosimetry File 99 (JENDL/D-99)[12].

As for $^{46}$Ti, the (n,2n) and (n,p) reaction cross sections were taken from JENDL/A-96. Figure 6 shows the evaluated cross sections for the (n,2n) reaction. The cross sections for the (n,d), (n,t), (n,$^3$He) and (n,2p) reactions on $^{46}$Ti were calculated with the EGNASH code.

The (n,np), (n,d), (n,t), (n,$^3$He) and (n,2p) reaction cross sections of $^{47}$Ti were obtained from the EGNASH calculations. The (n,p) cross section of $^{47}$Ti was taken from JENDL/D-99.

The (n,np) and (n,p) cross sections of $^{48}$Ti were taken from JEDNL/A-96. The (n,n$\alpha$), (n,d), (n,t), (n,$^3$He) and (n,2p) cross sections of $^{48}$Ti were calculated with the EGNASH code. The evaluated (n,np) cross section is shown in Fig. 7.

Concerning $^{50}$Ti, the (n,d), (n,t), (n,$^3$He) and (n,$\alpha$) cross sections were calculated with the EGNASH code.

### 4.4 Angular Distribution of Secondary Neutrons

The JENDL-3.2 data on the angular distributions of the elastically scattered neutrons for the Ti isotopes deviate abruptly from experimental ones in the energy region above 5 MeV. Therefore, these data were re-evaluated based on the calculations with the CASTHY code[13] using the modified Walter-Guss potential[8,14]. It is found from Fig. 8 that the present evaluation reproduces the measured angular distributions satisfactorily.

The data on the angular distributions of the inelastically scattered neutrons for the Ti isotopes were taken from JENDL-3.2.

### 4.5 Energy-angle Distribution of Secondary Particles

All the data on the energy-angle distributions for neutrons, protons and $\alpha$-particles were taken from JENDL/F-99[4].

### 4.6 Gamma-ray Production Data

Gamma-ray production data were obtained newly from theoretical calculations

for each Ti isotope. The calculations were made mainly with the EGNASH code[8] and the calculated data were compiled into the ENDF format[15] using the GAMFIL2 code[16]. The gamma-ray multiplicities and spectra due to a capture reaction were calculated with the CASTHY code[13]. As for $^{48}$Ti, the calculated spectra were replaced with the data measured by a group of the Tokyo Institute of Technology[17] between 18 and 134 keV. Isotropic angular distributions were assumed for emitted gamma-rays.

In making the data file, multiplicities of emitted gamma-rays were given except for the inelastic scattering to discrete levels. Transition probabilities were provided for the calculation of the (n,n'γ) cross sections due to discrete levels.

### 4.7 Covariance Data

The data on covariance were given only for $^{48}$Ti. The covariances of the total, total inelastic scattering, (n,2n), (n,nα), (n,np), (n,γ), (n,p) and (n,α) cross sections were obtained from available experimental data by using the GMA code[18].

## 5. Elemental Vanadium

Elemental vanadium contains two isotopes: $^{50}$V (0.250 %) and $^{51}$V (99.750 %). The contribution from $^{50}$V can be seen on the total, elastic scattering and capture cross sections of elemental vanadium below several keV, although no large contribution of $^{50}$V is expected for the remaining reactions on the element. Therefore, it was decided that the elemental data would be given in JENDL-3.3, since the low-energy resonance structure is important for applications. Except the total, elastic scattering and capture cross sections, the evaluated data were constructed only from the $^{51}$V component.

### 5.1 Resolved Resonance Parameters

Considering the resonance parameters given by Mughabghab et al.[19], the best-fit values were determined so as to reproduce the experimental data obtained by Brusegan et al.[20], Garg[21], Rohr&Friedland[22], Winters et all.[23] and Macklin&Winters[24] with the Reich-Moore formalism. A negative resonance was added to reproduce the thermal scattering and capture cross sections of $^{51}$V recommended by Mughabghab et al.[19] The contribution of $^{50}$V was calculated from the resonance parameters given in Ref. 19 and regarded as background cross sections in the data file. The evaluated total cross section is shown in Fig. 9.

### 5.2 Total, Elastic Scattering and Capture Cross Sections above the Resonance Region

The total cross sections between 100 and 250 keV were evaluated on the basis of the experimental data of Rohr&Friedland[22] and Smith et al.[25] Above 250 keV the latest measurements[26] were adopted, although the cross sections were averaged over a

half MeV interval above 5 MeV. The result is shown in Fig. 10.

The pre-equilibrium component of capture cross sections was calculated by using the GNASH code[10] above 1.5 MeV. The parameters required as input to the code are given as follows:

Optical potentials

Walter and Guss[14] for neutrons, Perey[27] for protons, Lohr and Haeberli[28] for deuterons, and Shepard et al.[29] for α-particles.

Level density parameters

Default values in EGNASH[8].

Gamma-ray transmission coefficients

Kopecky-Uhl type[30].

Giant-dipole resonance parameters

Dietrich and Berman[31].

Figure 11 depicts the evaluated capture cross sections.

The elastic scattering cross sections were obtained by subtracting a sum of the partial non-elastic cross sections from the total cross sections.

### 5.3 (n,np) Reaction Cross Section

The (n,np) cross sections were revised by adopting the values obtained from the systematics made by Manokhin[32].

### 5.4 Gamma-ray Production Data

The gamma-ray spectra and multiplicities were calculated by using the EGNASH code[8]. The pre-equilibrium gamma-ray emission was considered for the capture reaction by using the GNASH code[10]. The calculated capture gamma-ray spectra were replaced with the data measured by a group of the Tokyo Institute of Technology[17] below 559 keV.

### 5.5 Energy-angle Distribution of Secondary Particles

All the data on the energy-angle distributions for neutrons, protons, deuterons, tritons and α-particles were taken from JENDL/F-99[4].

### 5.6 Covariance Data

Covariances were estimated from the experimental data on the total, elastic scattering, capture, (n,2n), (n,p), and (n,α) cross sections by using the GMA code[18].

## 6. Chromium Isotopes

The data of the Cr isotopes were widely re-evaluated for JENDL-3.3. In the re-evaluation work, the JENDL-3.2 data were examined by considering new experimental data. The data on gamma production for all isotopes and the covariances for $^{52}$Cr were newly evaluated. Only the data modified and newly evaluated are described. The abundance of each isotope is tabulated below:

| Isotope | Abundance (%) |
|---|---|
| $^{50}$Cr | 4.345 |
| $^{52}$Cr | 83.789 |
| $^{53}$Cr | 9.501 |
| $^{54}$Cr | 2.365 |

### 6.1 Resolved Resonance Parameters

The resolved resonance parameters of the Cr isotopes in JENDL-3.2 were extensively revised. In order to make a better fit to experimental data, the resonance formula used were changed to the Reich-Moore type from the multi-level Breit-Wigner type. The parameter data for each level of the Cr isotopes were examined by comparing them with recent experimental data, and modified. The upper boundaries of the resonance regions for $^{50}$Cr, $^{52}$Cr, $^{53}$Cr and $^{54}$Cr were expanded to 600, 855, 245 and 750 keV from 300, 300, 120 and 300keV, respectively.

For $^{52}$Cr which is the most abundant isotope in the element, a further examination was made using the experimental data for natural Cr. The resonance parameters of $^{52}$Cr were adjusted so that the total cross sections calculated for the element could reproduce well the corresponding experimental ones. In order to obtain further agreement with the experimental total cross-section for the element, the background cross section was given for the total cross section of $^{52}$Cr. The results of the total cross sections for $^{52}$Cr and the Cr element are shown in Figs.12-16, together with experimental data and JENDL-3.2. The present evaluation improves the underestimate of the total cross sections of the element around 1 keV, as seen in Fig. 14.

### 6.2 Total, Elastic Scattering and Capture Cross Sections above the Resonance Region

In the energies above the resolved resonance region, the total cross sections for $^{50,53,54}$Cr isotopes were taken from JENDL-3.2. The total cross section of $^{52}$Cr was determined so that a sum of all isotopic contributions could reproduce measured total cross sections of the elemental Cr.

The pre-equilibrium components of the capture cross sections above the

resonance region were calculated with the GNASH code[10]. The pre-equilibrium cross sections obtained were added to the JENDL-3.2 data for the Cr isotopes. For example, the evaluated capture cross section of $^{52}$Cr is shown in Fig. 17.

The elastic scattering cross sections were given by subtracting a sum of the capture and the other non-elastic cross sections from the total cross sections.

### 6.3 Reaction Cross Sections

The threshold-reaction cross-sections were re-evaluated using the EGNASH code [8]. The cross sections for the (n,d), (n,t), (n,$^3$He) and (n,2p) reactions on each isotope were newly evaluated from the EGNASH calculations

As for $^{50}$Cr, the data on the (n,p), (n,np), (n,α) and (n,nα) reactions were revised. For example, the (n,p) cross section of $^{50}$Cr is shown in Fig.18.

For $^{52}$Cr, the cross sections for the (n,2n), (n,np), (n,α) and (n,nα) reactions were re-evaluated. Figures 19 and 20 show the cross sections for the (n,2n) reaction on $^{52}$Cr and on the element. As shown in Fig. 19, the (n,2n) cross section in JENDL-3.2 was evaluated on the basis of the experimental data of Bormann et al[33]. In the present evaluation, the calculation with the EGNASH code was made so as to reproduce well the experimental data of Liskien et al.[34] and Fessler et al.[35] It is found from Fig. 20 that the present and JENDL-3.2 evaluations agree with the data on the element measured by Frehaut et al.[36] below 15 MeV.

Concerning $^{53}$Cr, the data on the (n,p), (n,np) and (n,α) reactions were slightly modified.

### 6.4 Energy-angle Distribution of Secondary Particles

All the data on the energy-angle distributions for neutrons, protons and α-particles were taken from JENDL/F-99[4].

### 6.5 Gamma-ray Production Data

Gamma-ray production data were evaluated newly from theoretical calculations for each Cr isotope. The calculations were made mainly with the EGNASH code[8] and the calculated data were processed using the GAMFIL2 code[16].

In these data evaluations on gamma production, the gamma-ray spectra and the multiplicities for the emitted gamma-rays were calculated separately for each reaction. The transition probabilities were given for each discrete level in the inelastic scattering. The calculation with the CASTHY code[13] was made to obtain the gamma-ray spectra and the multiplicities due to a capture reaction. The calculated capture gamma-ray spectra between 31 and 545 keV were replaced with the experimental data of Igashira et al.[17] Isotropic angular distributions were assumed for emitted gamma-rays.

### 6.6 Covariance Data

The data on covariance were given only for $^{52}$Cr. Except for the (n,2n) reaction, the covariance data were taken from the JENDL-3.2 Covariance File[37]. The covariance data for the (n,2n) reaction on $^{52}$Cr were estimated on the basis of the experimental data with the GMA code[18].

## 7. Iron Isotopes

Some problems were pointed out by the shielding benchmark tests of the iron data in JENDL-3.2. In the present work, the total cross sections and resolved resonance parameters were mainly modified for $^{54}$Fe and $^{56}$Fe. Most of the covariance data from $^{56}$Fe were taken from the JENDL-3.2 Covariance File[37]. The abundance of each isotope is tabulated below:

| Isotope | Abundance (%) |
|---|---|
| $^{54}$Fe | 5.845 |
| $^{56}$Fe | 91.754 |
| $^{57}$Fe | 2.119 |
| $^{58}$Fe | 0.282 |

### 7.1 Resolved Resonance Parameters

The resolved resonance parameters for $^{54}$Fe and $^{56}$Fe were taken from ENDF/B-VI[38] and JEF-2.2[39], respectively. As a result, the upper boundaries of the resonance region were extended from 250 keV to 700 keV for $^{54}$Fe and to 850 keV for $^{56}$Fe. We adopted the Reich-Moore formula for all isotopes, although the parameters for $^{57,58}$Fe remained unchanged. Figures 21 and 22 illustrate the total cross sections of $^{54}$Fe and $^{56}$Fe, respectively.

### 7.2 Total Cross Sections above the Resonance Region

The total cross section of $^{54}$Fe was based on the measurements of Carlton et al.[40] in the energy region from 0.7 to 7.0 MeV. Above 7 MeV, the cross section was evaluated on the basis of a least-squares fit to the experimental data of Carlton et al.[40] and Cornelis et al.[41]

The total cross sections of $^{57,58}$Fe remain unchanged from JENDL-3.2. These cross sections were obtained from optical model calculations. The cross sections of elemental iron were derived from the experimental data[42-44] in the energy region from 0.7 to 20 MeV. Then, the cross section of $^{56}$Fe was obtained by subtracting the contributions of $^{54,57,58}$Fe from the cross section of elemental iron. Figure 23 shows the total cross section of elemental iron in the energy region from 1.0 to 1.1 MeV.

### 7.3 (n,2n) Cross Section

The (n,2n) cross section of $^{56}$Fe was re-calculated with the TNG code[45]. The parameters required as input to the code were taken from the work of Fu[46] for ENDF/B-VI. The resultant (n,2n) cross sections of $^{56}$Fe and of the element are shown in Figs. 24 and 25, respectively.

### 7.4 Capture Cross Sections and Gamma-ray Spectra

In JENDL-3.2, the direct-semi-direct (DSD) component was not taken into account, although the capture cross section of $^{58}$Fe was phenomenologically enhanced above 10 MeV. The pre-equilibrium capture cross sections calculated from the TNG code were added to the ones in JENDL-3.2 except $^{58}$Fe above 5 MeV.

The capture gamma-ray spectra for $^{56}$Fe were replaced with the data measured by Igashira et al.[17] between 27.5 and 570 keV.

### 7.5 Elastic Angular Distributions and Particle Emission Spectra

The elastic angular distributions for $^{56}$Fe were revised by using the optical model calculations with the potential parameters of Arthur and Young[47] above 10 MeV. The distributions for the rest of the isotopes remain unchanged.

Angle-dependent neutron and charged-particle emission spectra were taken from JENDL/F-99[4].

### 7.6 Covariance Data

The covariance data for $^{56}$Fe were taken from the JENDL-3.2 Covariance File[37] except for those of the total cross section. The covariances of the total cross section were estimated from the experimental data[42-44] by using the GMA code[18].

## 8. Cobalt-59

It was pointed out[48] that the JENDL-3.2 calculations could not reproduce the measured leakage neutron spectra from a spherical assembly of cobalt at 14 MeV. However, we concluded that there is no problem with the evaluated neutron emission spectra at 14 MeV by comparing them with the measured double-differential neutron emission spectra, as seen in Fig. 26.

### 8.1 Resolved Resonance Parameters

The resonance parameters were determined so as to reproduce the experimental data[21,49] below 100 keV with the Reich-Moore formalism. Negative-energy levels were added to reproduce the thermal cross sections recommended by Mughabghab et al.[19] The evaluated total cross section is illustrated in Fig. 27.

### 8.2 Total, Elastic Scattering and Capture Cross Sections above the Resonance Region

The total cross section was evaluated on the basis of the experimental data[49-51] above 100 keV. Figure 28 shows the total cross section in the energy region from 1.2 to 1.3 MeV.

The pre-equilibrium component of the capture cross section was calculated with the GNASH code[10] above 1.5 MeV. The parameters required as input to the code are the same as those given in Sect. 5.2.

The elastic scattering cross sections were obtained by subtracting a sum of the non-elastic partial cross sections from the total cross sections.

### 8.3 (n,2n) Cross Section

The (n,2n) cross section was taken from JENDL/A-96[11].

### 8.4 Gamma-ray Production Data

The gamma-ray spectra and multiplicities were calculated by using the EGNASH[8] code. The calculated capture gamma-ray spectra were replaced with the data measured by Igashira et al.[17] between 23 and 550 keV.

### 8.5 Energy-angle Distribution of Secondary Particles

All the data on the energy-angle distributions for neutrons, protons, deuterons and α-particles were taken from JENDL/F-99[4].

### 8.6 Covariance Data

Covariances were estimated from the experimental data on the total, elastic scattering, capture, (n,2n), (n,p), and (n,α) cross sections by using the GMA code[18].

## 9. Nickel Isotopes

The threshold-reaction cross sections of all isotopes were extensively re-evaluated by the EGNASH[8] calculations. The abundance of each isotope is tabulated below:

| Isotope | Abundance (%) |
|---|---|
| $^{58}$Ni | 68.077 |
| $^{60}$Ni | 26.223 |
| $^{61}$Ni | 1.140 |
| $^{62}$Ni | 3.634 |
| $^{64}$Ni | 0.926 |

### 9.1 Resolved Resonance Parameters

The resonance parameters of $^{58}$Ni were replaced with the values obtained by Perey et al.[52] below 812 keV. The resonance formula was changed to the

Reich-Moore formula from the Breit-Wigner one. The parameters for the other isotopes remain unchanged.

### 9.2 Total Cross Section above the Resonance Region

The total cross sections of $^{58,62}$Ni were taken from the experimental data on the natural element measured by Larson et al.[53] above 812 keV and 557 keV, respectively. As for $^{60}$Ni, the high resolution measurements of Perey et al.[54] were traced between 456 and 557 keV, while the data of Larson et al. were adopted above 557 keV. The cross section of $^{61}$Ni is based on the measurements of Cho et al.[55] between 57.0 and 74.6 keV, the JENDL-3.2 data between 74.6 and 1.5 MeV, and the data of Larson et al.[53] above 1.5 MeV. The cross section of $^{64}$Ni was obtained from the experimental data of Farrel et al.[56] between 553 and 557 keV and from the data of Larson et al.[53] above 557 keV.

### 9.3 Inelastic Scattering and Threshold Reaction Cross Sections

No change was made for the inelastic scattering cross sections of $^{58,60}$Ni. The inelastic scattering cross sections of $^{61,62,64}$Ni and other threshold reaction cross sections were calculated using the EGNASH code[8]. The evaluated $^{60}$Ni(n,p) cross section is illustrated in Fig. 29. In this reaction, the JENDL-3.2 evaluation is obviously based on the old measurements of Paulsen and Liskien[57], whereas the present evaluation reproduces the recent measurements.

### 9.4 Particle Emission Spectra

Double-differential particle emission spectra for $^{58,60}$Ni were taken from JENDL/F-99[4]. As for the remaining isotopes, the spectra of the MF5 type were calculated with the EGNASH code[8].

### 9.5 Gamma-ray Production Data

In JENDL-3.2, gamma-ray production data are available only for $^{58,60}$Ni. The present work undertook the evaluation of gamma-ray production data for the other isotopes by using the EGNASH code. As for the capture reaction on $^{58}$Ni, we adopted the gamma-ray spectra on the natural element measured by Igashira et al.[17] between 16 and 550 keV.

### 9.6 Covariance Data

The covariances for $^{58,60}$Ni were taken from the work of Shibata and Oh.[58]

## 10. Copper-63,65

It was pointed out[59] that the calculations based on JENDL-3.2 are inconsistent with the low energy portion of the neutron spectra measured at 14 MeV. We examined the resonance parameters of both isotopes and modified some parameters. However, these attempts were unsuccessful in improving the fit. Therefore, the resonance

parameters remain unchanged from JENDL-3.2.

The abundance of each isotope is tabulated below:

| Isotope | Abundance (%) |
|---|---|
| $^{63}$Cu | 69.17 |
| $^{65}$Cu | 30.83 |

### 10.1 Total Cross Sections above the Resonance Region

The total cross sections of $^{63,65}$Cu were evaluated on the basis of the elemental data measured by Foster, Jr. and Glasgow[50], Larson[60], Guenther et al.[61] and Finlay et al.[62] in the energy region from 1.4 to 20 MeV. The same data were used for both isotopes in this energy region, since there was no isotopic measurement available. Figure 30 shows the total cross section of the element.

### 10.2 Energy-angle Distribution of Secondary Particles

Double-differential neutron, proton, deuteron and α-particle emission spectra were taken from JENDL/F-99[4].

## 11. Niobium-93

In JENDL-3.2[1], a high-energy (n,γ) component due to direct capture was neglected in the gamma-ray energy spectrum (MF=15 and MT=102). The radiative capture cross section (MF=3 and MT=102) includes a direct capture component in JENDL-3.2, but the energy spectrum (MF=15 and MT=102) contains only a statistical component. Maekawa and Oyama[63] pointed out a discrepancy between their measured and calculated leakage gamma-ray spectra seen in high-energy region in the benchmark test with 14-MeV neutrons. Since the discrepancy may be partly due to the neglect of the direct capture component, the high-energy (n,γ) spectrum has been calculated using the GNASH code[10] in the present evaluation. The GNASH code can account for pre-equilibrium gamma-ray emission within the framework of the exciton model, which allows a simple estimate of the direct-semidirect capture energy spectrum.

Other cross sections and energy distributions except MT=102 were taken from JENDL-3.2[1] and JENDL/F-99[4].

### 11.1 Calculation of the Energy Spectrum of Direct Capture Reaction

The gamma-ray energy spectrum is defined by

$$\frac{d\sigma_\gamma}{dE'} = m\sigma_\gamma p(E \to E'), \qquad (1)$$

where $m$ is the multiplicity given in MF=12 and MT=102 and $\sigma_\gamma$ the capture cross section given in MF=3 and MT=102, and $p(E \to E')$ the normalized energy distribution stored in MF=15 and MT=102:

$$\int p(E \to E')dE' = 1. \tag{2}$$

The multiplicity $m$ is calculated using the maximum energy of capture gamma-ray, $E_\gamma^{max}$ and the average gamma-ray energy $\overline{E}_\gamma$ as follows:

$$m = E_\gamma^{max} / \overline{E}_\gamma, \tag{3}$$

and

$$\overline{E}_\gamma = \int E' p(E \to E')dE'. \tag{4}$$

Here let us divide $p(E \to E')$ into two components, a statistical component $p_s(E \to E')$ and a direct capture component, $p_d(E \to E')$:

$$p(E \to E') = c_s p_s(E \to E') + c_d p_d(E \to E'), \tag{5}$$

where $c_s$ and $c_d$ denote a fraction of each component, respectively and have the following relation:

$$c_s + c_d = 1. \tag{6}$$

The energy distributions, $p_s(E \to E')$ and $p_d(E \to E')$, are normalized as in Eq. (2).

Next, inserting Eqs. (4) and (5) into Eq. (3), one can rewrite the multiplicity in the following:

$$m = \frac{E_\gamma^{max}}{c_s \int E' p_s(E \to E')dE' + c_d \int E' p_d(E \to E')dE'} = \frac{E_\gamma^{max}}{c_s \overline{E}_\gamma^s + c_d \overline{E}_\gamma^d}, \tag{7}$$

where $\overline{E}_\gamma^s$ and $\overline{E}_\gamma^d$ are the average gamma-ray energies for the statistical and direct capture components and calculated with Eq.(4).

Here, we define the cross section of direct capture process as $\sigma^{dir}$. From Eqs. (1) and (5),

$$\sigma^{dir} = \int \frac{d\sigma^{dir}}{dE'} dE' = m\sigma_\gamma c_d \ . \tag{8}$$

By solving a set of the equations (6) to (8) with respect to $m$, $c_s$, and $c_d$, we can obtain two physical quantities to be put in the file, i.e., $p(E \to E')$ and $m$. It should be noted that the energy balance holds in the above calculation, because Eq.(3) is satisfied.

In the present JENDL-3.3 evaluation, we have used the same total capture cross sections $\sigma_\gamma$ as in JENDL-3.2 and have assumed that the statistical component $p_s(E \to E')$ is the same as $p(E \to E')$ in JENDL-3.2. The direct component $\sigma^{dir}$ and $p_d(E \to E')$ were calculated using the GNASH code. Input parameters used in the GNASH calculation were basically the same as used in JENDL-3.2 evaluation,

the GNASH calculation were basically the same as used in JENDL-3.2 evaluation, except that the neutron optical potential of Wilmore-Hodgson.[64] was used in the present work. Since the calculated direct component was very small at low incident energies, the direct component was added for incident neutron energies above 3 MeV. The calculated energy spectrum of the direct capture component was normalized to an experimental data[65] for 14 MeV, and the normalization factor was also used for other incident energies.

The (n,γ) spectra of JENDL-3.3 are compared with those of JENDL-3.2 and the experimental data[65] in Fig. 31. The solid lines and the dotted lines correspond to JENDL-3.3 and JENDL-3.2, respectively. It is found that inclusion of the direct capture component leads to an increase in the cross sections in the high-energy part of the energy spectrum and results in good agreement with the experimental data at 14 MeV.

The multiplicity $m$ (MF=12 and MT=102) calculated with Eq.(7) are plotted in Fig. 32 together with that of JENDL-3.2 as a function of incident neutron energy. The multiplicity is reduced by inclusion of the direct component at energies above 5 MeV. This reduction can be explained from Eq.(7) by the increase in high-energy gamma-ray released via the direct capture process.

### 11.2 Comments on Secondary Neutron Spectra

Ichihara et al.[66] have recently reported a sensitivity analysis of measured leakage neutron spectra from a spherical pile of Nb bombarded with 14 MeV neutrons using MCNP-4A and JENDL-3.2 and showed that the MCNP calculation with JENDL-3.2 gives satisfactory prediction except below 0.8 MeV. They have also pointed out that there may be a problem on the secondary energy distribution of the (n,2n) reaction in JENDL-3.2 for the discrepancy seen below 0.8 MeV, and 20% reduction of the (n,2n) cross section and a modification of the shape of the energy distribution are required to improve the discrepancy between the measurement and the calculation. However, the (n,2n) data of JENDL-3.2 were adopted again in JENDL-3.3, from the following reasons: there is currently no experimental secondary energy spectrum data to be compared directly with the evaluated one at very low emission energies below 0.8 MeV and 20% reduction of the (n,2n) cross section in JENDL-3.2 is too large to be accepted in comparisons with available experimental data. Further efforts will be needed to resolve this (n,2n) problem consistently between differential data and integral tests in the future.

## 12. Tungsten Isotopes

The data of the W isotopes for JENDL-3.2 were partly re-evaluated for JENDL-3.3. In the re-evaluation, the JENDL-3.2 data were examined by considering new experimental ones and updated. The data on gamma production were newly evaluated. The abundance of each isotope is tabulated below:

| Isotope | Abundance (%) |
|---|---|
| $^{180}$W | 0.12 |
| $^{182}$W | 26.50 |
| $^{183}$W | 14.31 |
| $^{184}$W | 30.64 |
| $^{186}$W | 28.43 |

JENDL-3.3 does not contain the data for $^{180}$W, since its contribution is negligible.

### 12.1 Resolved Resonance Parameters

The resolved resonance parameters for each W isotope were taken from the JENDL-3.2 file[1] except only for the parameters of $^{186}$W. The radiative capture width of the 18.8-eV resonance for $^{186}$W was changed to 52 meV from 30 meV and a negative resonance was deleted. As a result, the calculated resonance integral, 529 b, is consistent with a value of 510.7±24.3 b measured by Kobayashi et al.[67] In Fig. 33, the revised data on the total cross section of $^{186}$W are shown together with the JENDL-3.2 data and the experimental ones. Figure 34 shows the capture cross section of $^{186}$W by comparing with the JENDL-3.2 data and the experimental ones.

### 12.2 Threshold Reaction Cross Sections

Most of the threshold-reaction cross sections of the W isotopes were taken from JENDL-3.2 except a few reactions described hereafter. In order to make a good fit to the experimental data, the (n,2n) reaction cross sections of $^{183}$W and $^{186}$W were revised using the EGNASH code[8]. Figures 35 and 36 show the revised (n,2n) cross sections for $^{183}$W and $^{186}$W, respectively. As a result, the calculated (n,2n) cross sections of the element are in better agreement with the experimental data than the JENDL-3.2 ones, as seen in Fig. 37. The (n,np) reaction cross sections of $^{183}$W were also re-evaluated with the EGNASH code.

### 12.3 Energy-angle Distribution of Secondary Particles

All the data on the energy-angle distributions for neutrons, protons, deuterons and α-particles were taken from JENDL/F-99[4].

### 12.4 Gamma-production Data

All the data on gamma production were evaluated newly from theoretical calculations for each W isotope. The calculations were made mainly with the

EGNASH code[8] and the calculated data were processed using the GAMFIL2 code[16].

In making the data files, the gamma-ray production data were compiled for each reaction separately. For the inelastic scattering, the transition probabilities were given for each discrete level. Only for neutron capture, the gamma-ray production data were calculated with the CASTHY code[13]. Angular distributions of emitted gamma-rays were assumed to be isotropic

## 13. Other Data

The data with minor modifications are described in this section together with the results which were already published.

### 13.1 Fluorine-19

Double-differential neutron, proton, deuteron, triton, and α-particle were taken from JENDL/F-99[4].

### 13.2 Sodium-23

The resonance parameters remain unchanged from JENDL-3.2. Above the resonance region, re-evaluation was performed[68] on the basis of nuclear model calculations. The details of the evaluation are described in Ref. 68. The covariances were taken from the JENDL-3.2 Covariance File[37].

### 13.3 Magnesium Isotopes

Above 520 keV, the total cross section of $^{24}$Mg was taken from the elemental data of JENDL-3.2 after subtracting the $^{25,26}$Mg contributions. Gamma-ray production data of all isotopes were calculated with the EGNASH[8] and CASTHY[13] codes. As for the capture gamma-ray spectra for $^{24}$Mg, the calculations were replaced with the data measured by a group of the Tokyo Institute of Technology[17] between 44 and 430 keV. The abundance of each isotope is tabulated below:

| Isotope | Abundance (%) |
|---|---|
| $^{24}$Mg | 78.99 |
| $^{25}$Mg | 10.00 |
| $^{26}$Mg | 11.01 |

### 13.4 Phosphorus-31

The (n,p) reaction cross section was taken from JENDL/D-99[12]. The elastic scattering cross section was obtained by subtracting the non-elastic cross section from the total cross section.

### 13.5 Sulphur Isotopes

Gamma-ray production data were calculated with the EGNASH and CASTHY codes. The abundance of each isotope is tabulated below:

| Isotope | Abundance (%) |
|---|---|
| $^{32}$S | 95.02 |
| $^{33}$S | 0.75 |
| $^{34}$S | 4.21 |
| $^{36}$S | 0.02 |

### 13.6 Potassium Isotopes

Gamma-ray production data were calculated with the EGNASH and CASTHY codes. The abundance of each isotope is tabulated below:

| Isotope | Abundance (%) |
|---|---|
| $^{39}$K | 93.2581 |
| $^{40}$K | 0.0117 |
| $^{41}$K | 6.7302 |

### 13.7 Calcium Isotopes

Above 500 keV, the total cross section of $^{40}$Ca is based on the elemental data measured by Cierjacks et al.[69] and Foster, Jr. and Glasgow[50]. The JENDL-3.2 data were used to subtract the other isotopic contributions from the elemental data. Double-differential neutron, proton and α-particle spectra for all isotopes were taken from JENDL/F-99. Gamma-ray production data were calculated with the EGNASH and CASTHY codes. As for the capture gamma-ray spectra for $^{40}$Ca, the calculations were replaced with the data measured by a group of the Tokyo Institute of Technology[17] between 24 and 543 keV. The abundance of each isotope is tabulated below:

| Isotope | Abundance (%) |
|---|---|
| $^{40}$Ca | 96.941 |
| $^{42}$Ca | 0.647 |
| $^{43}$Ca | 0.135 |
| $^{44}$Ca | 2.086 |
| $^{46}$Ca | 0.004 |
| $^{48}$Ca | 0.187 |

### 13.8 Manganese-55

Double-differential neutron, proton, deuteron, triton, $^{3}$He and α-particle spectra were taken from JENDL/F-99. Concerning the capture gamma-ray spectra, the JENDL-3.2 data were replaced with the measurements obtained by a group of the Tokyo Institute of Technology[17] between 14 and 559 keV.

### 13.9 Arsenic-75

Double-differential neutron, proton, deuteron and α-particle spectra were taken

from JENDL/F-99.

### 13.10 Zirconium Isotopes

The data on the naturally-occurring isotopes of elemental zirconium were partly re-evaluated. Above the resonance region, the total cross sections of all isotopes were taken from the elemental data of JENDL-3.2. The isotopic capture cross sections were modified so as to reproduce the elemental data measured by Stavisskij et al.[70] and Poenitz[71].

Double-differential neutron, proton, deuteron, triton, $^{3}$He, and α-particle spectra were taken from JENDL/F-99. Gamma-ray production data were calculated with the EGNASH and CASTHY codes.

Covariances for the total inelastic scattering, (n,2n) and capture cross sections were obtained[72] on the basis of experimental data.

The abundance of each isotope is tabulated below:

| Isotope | Abundance (%) |
|---|---|
| $^{90}$Zr | 51.45 |
| $^{91}$Zr | 11.22 |
| $^{92}$Zr | 17.15 |
| $^{94}$Zr | 17.38 |
| $^{96}$Zr | 2.80 |

### 13.11 Molybdenum Isotopes

The data on the naturally-occurring isotopes were re-evaluated. Above the resonance region, the total cross sections of all isotopes were taken from the elemental data of JENDL-3.2. Double-differential neutron, proton, deuteron, triton, $^{3}$He, and α-particle spectra were taken from JENDL/F-99.

In the energy region above 420 keV, the gamma-ray production data of all isotopes were taken from the elemental data of JENDL-3.2, which are based on the empirical formula of Howerton and Plechaty[73]. Below 420 keV, the gamma-ray production data due to a capture reaction were calculated for each isotope with the CASTHY code. As for $^{95}$Mo, a multiplicity of 1.0 was set for the decaying gamma-ray from the 204.1-keV state below 420 keV, since it is not included in the CASTHY calculations.

The inelastic scattering cross sections were re-evaluated[74] for the low-lying levels of $^{92,98,100}$Mo: 1.5095-MeV state of $^{92}$Mo, 0.7384-, 0.7874-, 1.4323-, 1.5100-MeV states of $^{98}$Mo, and 0.5356-, 0.6944-, 1.0637-MeV states of $^{100}$Mo.

The isotopic abundance of each isotope is tabulated below:

| Isotope | Abundance (%) |
|---|---|
| $^{92}$Mo | 14.84 |
| $^{94}$Mo | 9.25 |
| $^{95}$Mo | 15.92 |
| $^{96}$Mo | 16.68 |
| $^{97}$Mo | 9.55 |
| $^{98}$Mo | 24.13 |
| $^{100}$Mo | 9.63 |

### 13.12 Cadmium Isotopes

Elemental cadmium consists of the following isotopes:

| Isotope | Abundance (%) |
|---|---|
| $^{106}$Cd | 1.25 |
| $^{108}$Cd | 0.89 |
| $^{110}$Cd | 12.49 |
| $^{111}$Cd | 12.80 |
| $^{112}$Cd | 24.13 |
| $^{113}$Cd | 12.22 |
| $^{114}$Cd | 28.73 |
| $^{116}$Cd | 7.49 |

There exists a problem with the Cd data in JENDL-3.2. In JENDL-3.2, the elemental data were produced after isotopic evaluations were finished. However, the scattering radius for the resolved resonances was changed to a value of 6.2 fm so that the measured thermal cross sections of the element could be reproduced. Moreover, in the energy region above the resolved resonance, the elemental total and capture cross sections were modified so as to reproduce the measured data. These modifications were not reflected on the isotopic evaluations. Therefore, there is inconsistency between the isotopic and elemental data in JENDL-3.2. In JENDL-3.3 where the elemental data were not produced, we adopted a value of 6.2 fm for the scattering radius of all the naturally-occurring isotopes in the resolved resonance region. In the unresolved resonance region 10-100 keV, background cross sections were given by considering the measured capture cross sections[71,75]. The total cross section of each isotope was taken from the elemental data in JENDL-3.2 above 100 keV.

Gamma-ray production data were evaluated with the EGNASH and CASTHY codes.

### 13.13 Antimony Isotopes

Elemental antimony consists of two isotopes. The isotopic abundance is tabulated below:

| Isotope | Abundance (%) |
|---|---|
| $^{121}$Sb | 57.21 |
| $^{123}$Sb | 42.79 |

Double-differential neutron, proton, deuteron, triton and α-particle spectra were taken from JENDL/F-99.

### 13.14 Europium Isotopes

Elemental europium consists of two isotopes:

| Isotope | Abundance (%) |
|---|---|
| $^{151}$Eu | 47.81 |
| $^{153}$Eu | 52.19 |

Gamma-ray production data were evaluated with the EGNASH and CASTHY codes.

### 13.15 Erbium Isotopes

Elemental erbium consists of the following isotopes:

| Isotope | Abundance (%) |
|---|---|
| $^{162}$Er | 0.139 |
| $^{164}$Er | 1.601 |
| $^{166}$Er | 33.503 |
| $^{167}$Er | 22.869 |
| $^{168}$Er | 26.978 |
| $^{170}$Er | 14.910 |

Evaluations were performed by using statistical-model codes. In the evaluations, we considered the capture cross sections of $^{166,167,168,170}$Er measured by a group of the Tokyo Institute of Technology[76]. The details of the evaluations will be given elsewhere[77].

### 13.16 Tantalum-181

The (n,α) reaction cross section was set to zero values below 500 keV, since an abnormal enhancement was seen below 500 keV in JENDL-3.2. The elastic scattering cross section was obtained by subtracting the non-elastic cross section from the total cross section.

### 13.17 Mercury Isotopes

Elemental mercury consists of the following isotopes:

| Isotope | Abundance (%) |
|---|---|
| $^{196}$Hg | 0.15 |
| $^{198}$Hg | 9.97 |
| $^{199}$Hg | 16.87 |
| $^{200}$Hg | 23.10 |
| $^{201}$Hg | 13.18 |
| $^{202}$Hg | 29.86 |
| $^{204}$Hg | 6.87 |

The evaluation is mainly based on nuclear model calculations. The details of the evaluation are given in Ref. 78.

### 13.18 Lead Isotopes

Elemental lead consists of the following isotopes:

| Isotope | Abundance (%) |
|---|---|
| $^{204}$Pb | 1.4 |
| $^{206}$Pb | 24.1 |
| $^{207}$Pb | 22.1 |
| $^{208}$Pb | 52.4 |

Double-differential neutron, proton and α-particle spectra for all isotopes were taken from JENDL/F-99. As for $^{206,207,208}$Pb, the gamma-ray production data due to the (n,n') and (n,2n) reactions were re-evaluated with the EGNASH code. The direct/semi-direct process was considered in a phenomenological way[79] for the capture cross sections of $^{206,207}$Pb.

The total cross section of $^{208}$Pb was replaced with the elemental data measured by Schwartz et al.[80] between 1 and 15 MeV.

### 13.19 Bismuth-209

Double-differential neutron, proton, deuteron and α-particle spectra were taken from JENDL/F-99. The capture cross sections were modified between 200 keV and 3 MeV by considering the recent measurements[81].

## 14. Concluding Remarks

Evaluations of neutron nuclear data for medium-heavy nuclides were performed for JENDL-3.3 by the Medium-heavy Nuclide Data Evaluation Working Group in JNDC to resolve the problems found in JENDL-3.2. Recent experimental data and model calculations were taken into account to produce reliable nuclear data for many applications.

**Acknowledgments**

The authors would like to thank all the members of JNDC for helpful comments and discussion.

**References**


1) T. Nakagawa et al.: *J. Nucl. Sci. Technol.*, **32**, 1259 (1995).
2) K. Shibata et al.: *J. Nucl. Sci. Technol.*, **39**, 1125 (2002).
3) F. Maekawa: "Nuclear Data Test with Gamma-ray Integral Experiments," JAERI-Conf 96-005, p.92 (1996).
4) S. Chiba et al.: *J. Nucl. Sci. Technol.*, **39**, 187 (2002).
5) M. Baba et al.: "Double-differential Neutron Emission Spectra for Al, Ti, V, Cr, Mn, Fe, Ni, Cu, and Zr," *Proc. Int. Conf. Nuclear Data for Science and Technology*, 1988 Mito, p.291 (1988).
6) P.D. Kunz and E. Rost: "The Distorted-wave Born Approximation," Computational Nuclear Physics 2, edited by K. Langanke, J.A. Maruhn, S.E. Koonin, Springer-Verlag, p.88 (1993).
7) IAEA: "Handbook for Calculations of Nuclear Reaction Data Reference Input Parameter Library," IAEA-TECDOC-1034, (1998).
8) N. Yamamuro: "A Nuclear Cross Section Calculation System with Simplified Input-format Version II (SINCROS-II)," JAERI-M 90-006 (1990).
9) J. Raynal: "Optical Model and Coupled-channel Calculations in Nuclear Physics," ICTP International Seminar Course, Trieste 1971, p.281 (1972).
10) P.G. Young et al.: "Comprehensive Nuclear Model Calculations: Introduction to the Theory and Use of the GNASH code," LA-12343-MS (1992).
11) Y. Nakajima: "Status of the JENDL Activation File," JAERI-Conf 96-008, p.50 (1996).
12) K. Kobayashi et al.: "JENDL Dosimetry File 99 (JENDL/D-99)," JAERI 1344 (2002).
13) S. Igarasi and T. Fukahori: "Program CASTHY – Statistical Model Calculation for Neutron Cross Sections and Gamma Ray Spectrum," JAERI 1321 (1991).
14) R.L. Walter and P.P. Guss: *Proc. Int. Conf. Nuclear Data for Basic and Applied Science*, Santa Fe 1985, p.1079 (1986).
15) Cross Section Evaluation Working Group: "ENDF-102 Data Formats and Procedures for the Evaluated Nuclear Data File ENDF-6," BNL-NCS-44945-01/04-Rev., (2001).
16) K. Hida: "GAMFIL: A Computer Program for Generating Photon Production Nuclear Data File," JAERI-M 86-150 (1986) [in Japanese].
17) M. Igashira et al.: Private communication (1999).
18) W.P. Poenitz: *Proc. Conf. Nuclear Data Evaluation Methods and Procedures*, BNL 1980, BNL-NCS-51363, p.249 (1981).

19) S.F. Mughabghab et al.: "Neutron Cross Sections," Vol.1, Part A, Academic Press (1981).
20) A. Brusegan et al.: "Neutron Total Cross Section of Vanadium," *Proc. Int. Conf. Nuclear Data for Science and Technology*, Trieste 1997, p.410 (1997).
21) J.B. Garg: *Nucl. Sci. Eng.*, **65**,76 (1978).
22) G. Rohr and E. Friedland: *Nucl. Phys.*, **A104**, 1 (1967).
23) R.R. Winters et al.: *Phys. Rev.*, **C18**, 2092 (1978).
24) R.L. Macklin and R.R. Winters: *Nucl. Sci. Eng.*, **78**, 110 (1981).
25) A.B. Smith et al.: *Phys. Rev.*, **C1**, 581 (1970).
26) G. Rohr et al.: Taken from EXFOR (1995).
27) F.G. Perey: *Phys. Rev.*, **131**, 745 (1963).
28) J.M. Lohr and W. Haeberli: *Nucl. Phys.*, **A232**, 381 (1974).
29) J.R. Shepard et al.: *Nucl. Phys.*, **A275**, 189 (1977).
30) J. Kopecky and M. Uhl: *Phys. Rev.*, **C41**, 1941 (1990).
31) S.S. Dietrich and B.L. Berman: *Atomic Data and Nuclear Data Tables*, **38**, 199 (1988).
32) V.N. Manokhin: "Some Criteria Selection of Evaluated Threshold Reaction Excitation Functions," INDC(CCP)-397 (1997).
33) M. Bormann et al.: *Nucl. Phys.*, **A115**, 309 (1968).
34) H. Liskien et al.: Taken fromEXFOR (1989).
35) A. Fessler et al.: *Phys. Rev.*, **C58**, 996 (1998).
36) J. Frehaut et al.: Taken from EXFOR (1980).
37) K. Shibata et al.: *J. Nucl. Sci. Technol.*, **Suppl. 2**, 40 (2002).
38) Cross Section Evaluation Working Group: "ENDF/B-VI Summary Documentation," BNL-NCS-17541 (ENDF-201), (1991).
39) C. Nordborg and M. Salvatores: "Status of the JEF Evaluated Data Library," *Proc. Int. Conf. Nuclear Data for Science and Technology*, Gatlinburg 1994, Vol. 2, p.680 (1994).
40) R.F. Carlton et al.: *Bull. Am. Phys. Soc.*, **30**, 1252 (1985).
41) E. Cornelis et al.: *Proc. Int. Conf. Nuclear Data for Science and Technology*, Antwerp 1982, p.135 (1983).
42) A.D. Carlson and R.J. Cerbone: *Nucl. Sci. Eng.*, **42**, 28 (1970).
43) F.G. Perey et al.: ORNL-4823 (1972).
44) K. Berthold et al.: *Proc. Int. Conf. Nuclear Data for Science and Technology*, Gatlinburg 1994, Vol. 1, p.218 (1994).
45) C.Y. Fu: ORNL/TM-7042 (1980); K. Shibata and C.Y. Fu: ORNL/TM-10093

(1986).
46) C.Y. Fu: Private communication (1985).
47) E.D. Arthur and P.G. Young: LA-8626-MS (1980).
48) C. Ichihara et al.: *Proc. The Third Specialists' Meeting on Nuclear Data for Fusion Reactor*, JAERI-Conf 96-005, p.80 (1996)..
49) G. de Saussure et al.: *Ann. Nucl. Energy*, **19**, 393 (1992).
50) D.G. Foster, Jr. and D.W. Glasgow: *Phys. Rev.*, **C3**, 576 (1971).
51) S. Cierjacks et al.: KfK-1000, Suppl. 2, (1969).
52) C.M. Perey et al.: ORNL/TM-10841 (1988).
53) D.C. Larson et al.: ORNL/TM-8203 (1983).
54) C.M. Perey et al.: ORNL/TM-5893 (1982).
55) M. Cho et al.: *Proc. Second Int. Conf. Nuclear Data for Reactors*, Helsinki 1970, Vol. 1, p.619 (1970).
56) J.A. Farrel et al.: *Ann. Phys.*, **37**, 367 (1966).
57) A. Paulsen and H. Liskien: *Nucleonik*, **10**, 91 (1967).
58) K. Shibata and S.Y. Oh: "Estimation of Covariances of Cr and Ni Neutron Nuclear Data in JENDL-3.2," JAERI-Research 2000-007 (2000).
59) F. Maekawa: Private communication (1996).
60) D.C. Larson: *Proc. Symp. Neutron Cross-sections from 10 to 50 MeV*, BNL-NCS-51245, p.277 (1980).
61) P. Guenther et al.: *Nucl. Phys.*, **A448**, 280 (1986).
62) R.W. Finlay et al.: *Phys. Rev.*, **C47**, 237 (1993).
63) F. Maekawa and Y. Oyama: *Nucl. Sci. Eng.*, **123**, 272 (1996).
64) D. Wilmore and P.E. Hodgson: *Nucl. Phys.*, **A166**, 231 (1971).
65) F. Rigaud et al.: *Nucl. Phys.*, **A173**, 551 (1971).
66) C. Ichihara et al.: *J. Nucl. Sci. Technol.*, **38**, 959 (2001).
67) K. Kobayashi et al.: *Proc. Conf. Neutron Physics*, Kiev 1987, Vol. 4, p.238 (1988).
68) K. Shibata: *J. Nucl. Sci. Technol.*, **39**, 1065 (2002).
69) S. Cierjacks et al.: KfK-1000 (1968).
70) Ju.Ja. Stavisskij et al.: *At. Energija*, **15**, 323 (1963).
71) W.P. Poenitz: ANL-83-4, p.239 (1982).
72) K. Shibata et al.: JAERI-Research 96-041 (1996) [in Japanese].
73) S.T. Howerton and E.F. Plechaty: *Nucl. Sci. Eng.*, **32**, 178 (1968).
74) T. Kawano et al.: *J. Nucl. Sci. Technol.*, **35**, 519 (1998).
75) D. Kompe: *Nucl. Phys.*, **A133**, 513 (1969).
76) A.K.M. Harun-ar-Rashid: Ph.D. Thesis, Tokyo Institute of Technology (2000);

A.K.M. Harun-ar-Rashid et al.: *J. Nucl. Sci. Technol.*, 37, 421 (2000); M. Igashira: Private communication (2002).

77) A.K.M. Harun-ar-Rashid et al.: To be published.

78) K. Shibata et al.: *J. Nucl. Sci. Technol.*, 34, 1171 (1997).

79) V. Benzi and G. Reffo: CCDN-NW/10 (1969).

80) R.B. Schwartz et al.: NBS-MONO-138 (1974).

81) K. Saito et al.: "Measurement of Cross Sections of the $^{210}$Po Production Reaction by keV-Neutron Capture of $^{209}$Bi," JAERI-Conf 2003-006, p. 133 (2003).

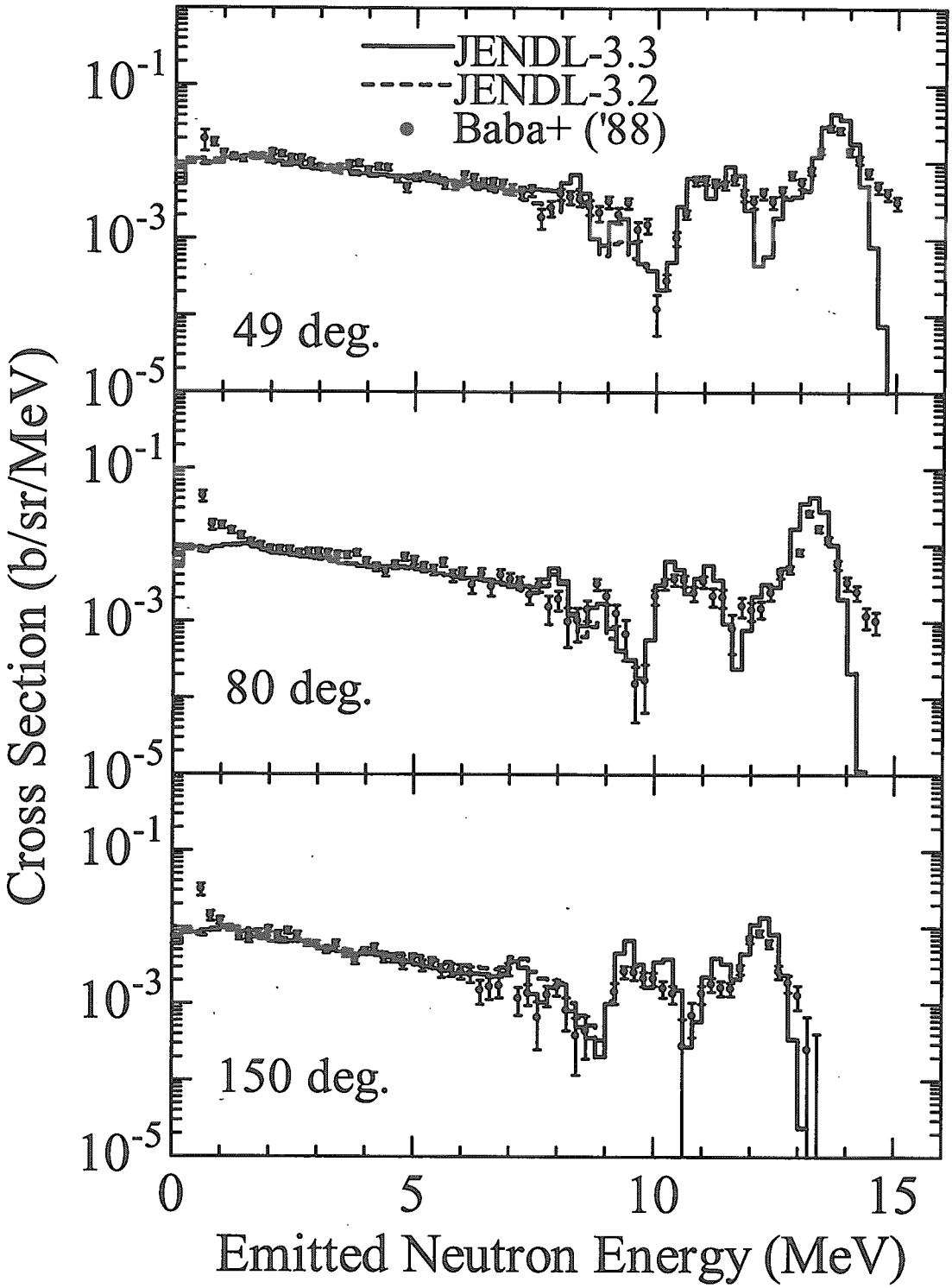


Fig. 1 Neutron emission spectra from $^{27}$Al at 14 MeV.

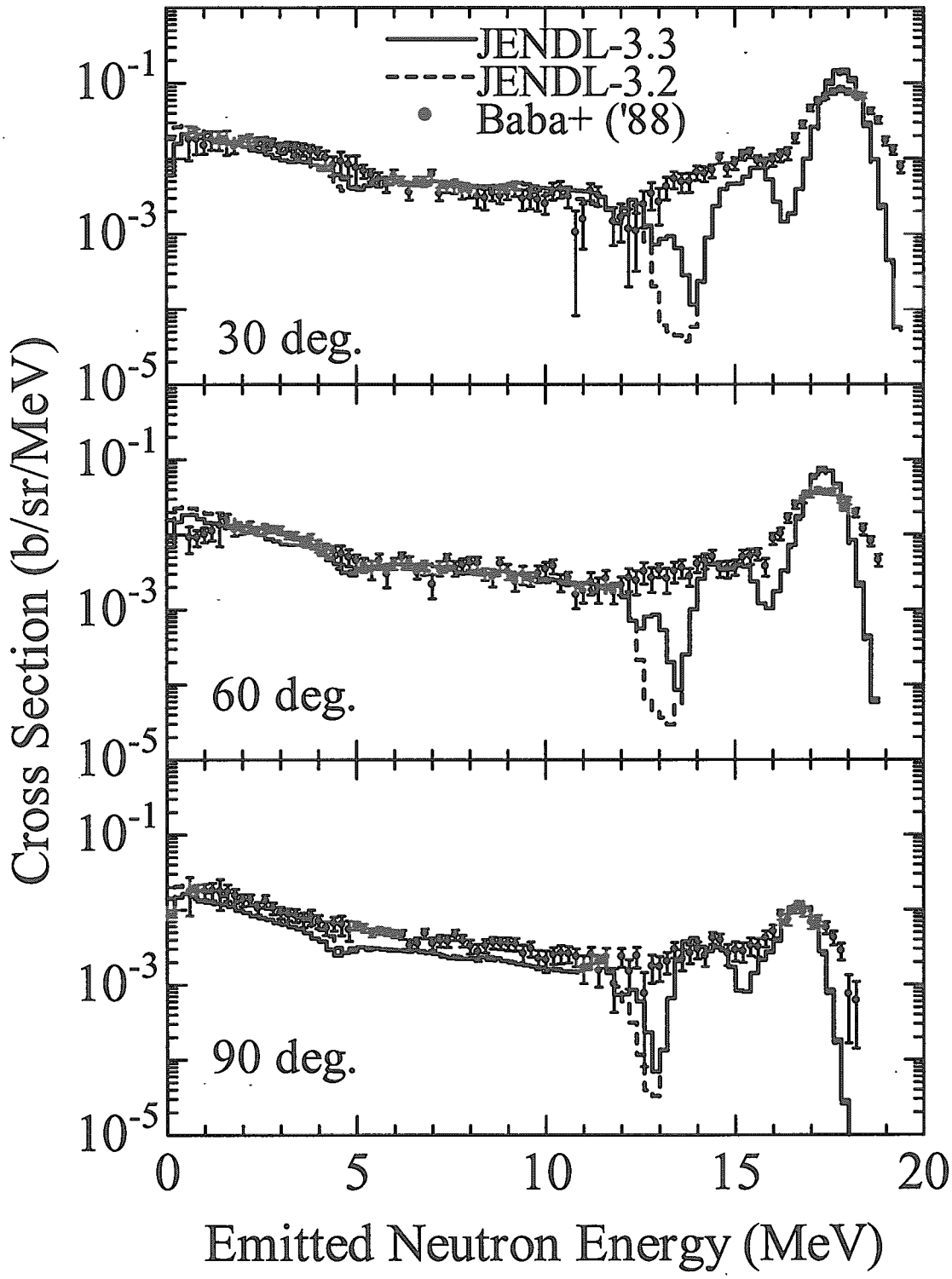


Fig. 2 Neutron emission spectra from $^{27}$Al at 18 MeV.

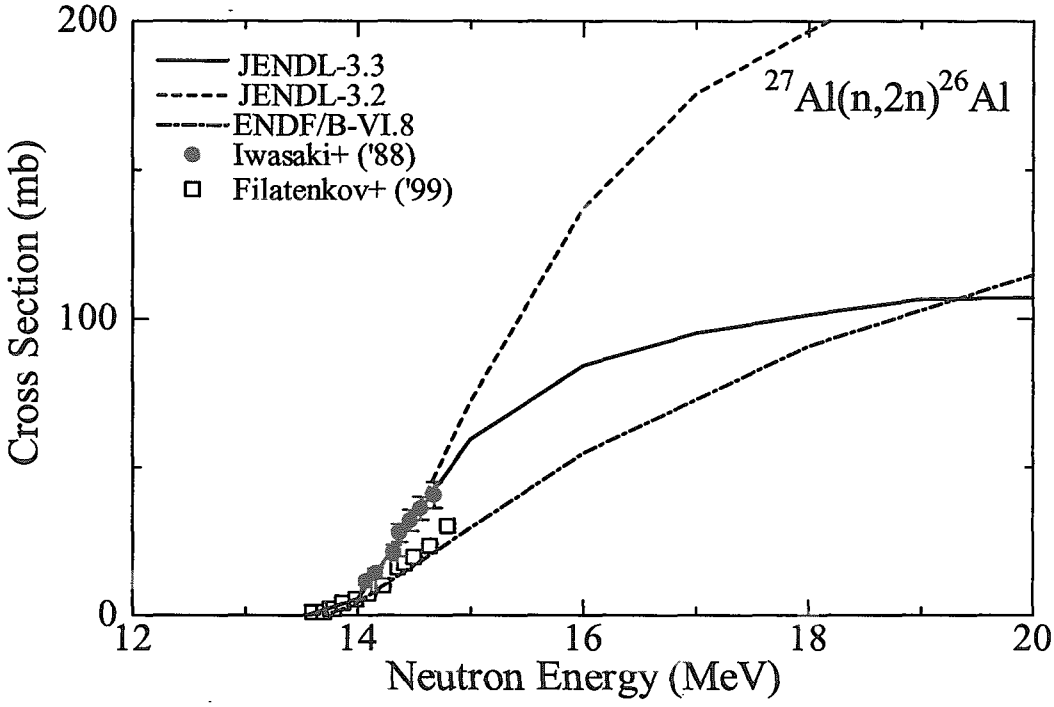


Fig. 3 $^{27}$Al(n,2n) cross section.

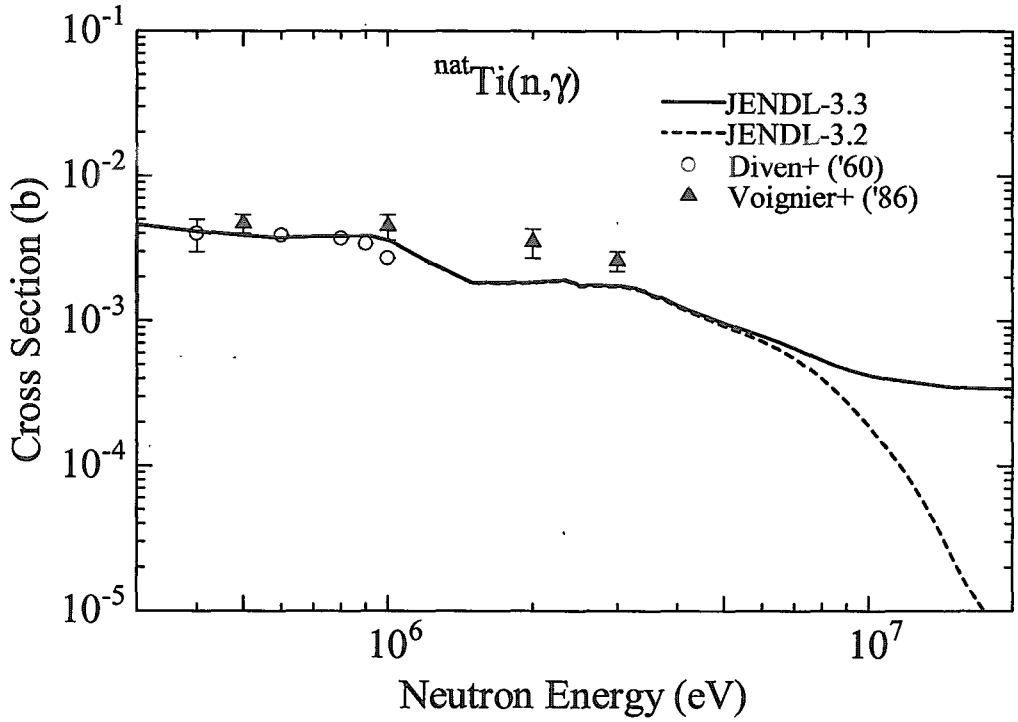


Fig. 4 Capture cross section of elemental Ti.

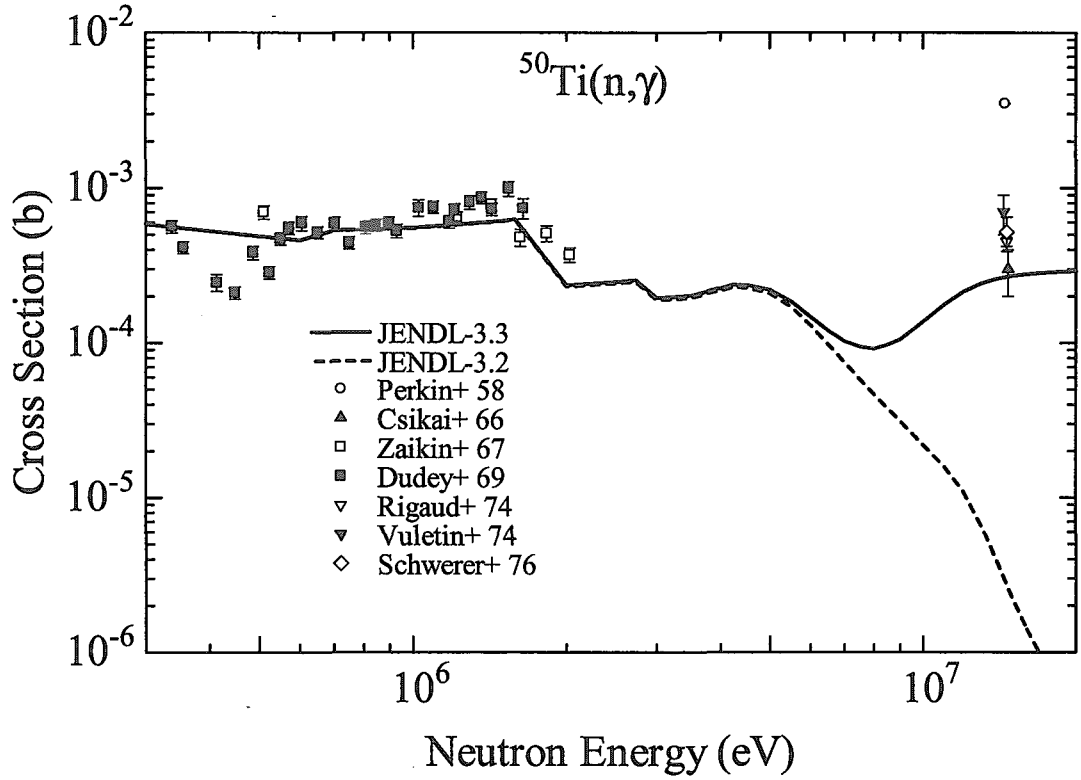


Fig. 5 Capture cross section of $^{50}$Ti.

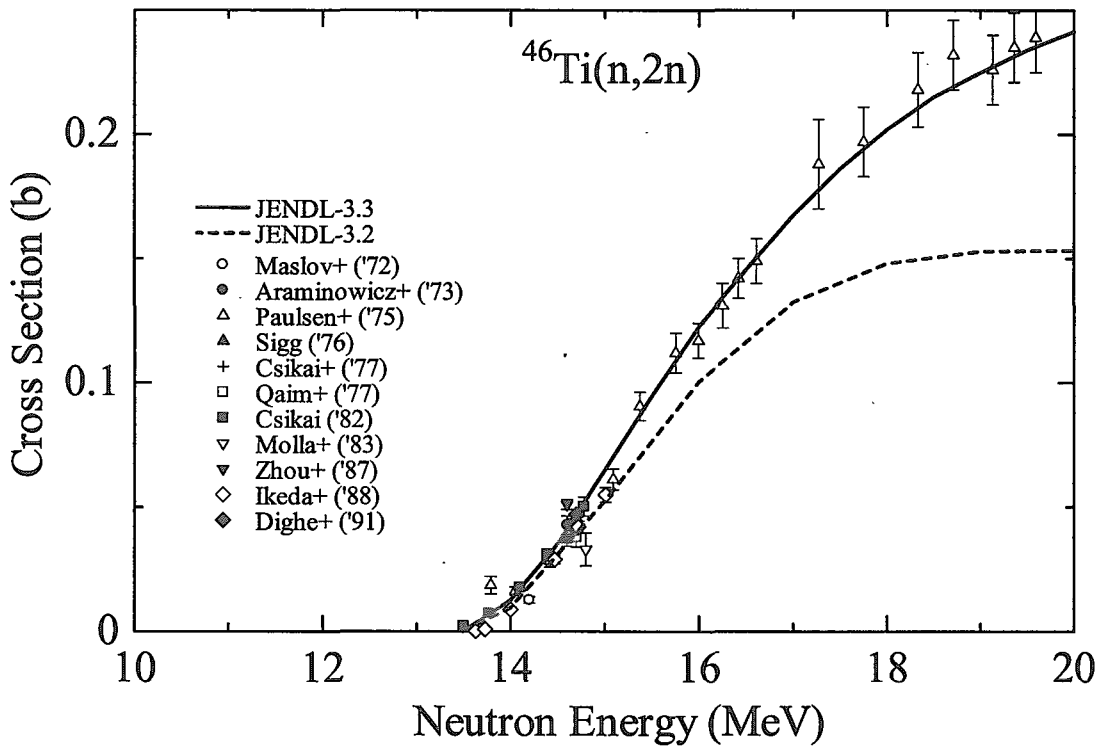


Fig. 6 $^{46}$Ti(n,2n) cross section.

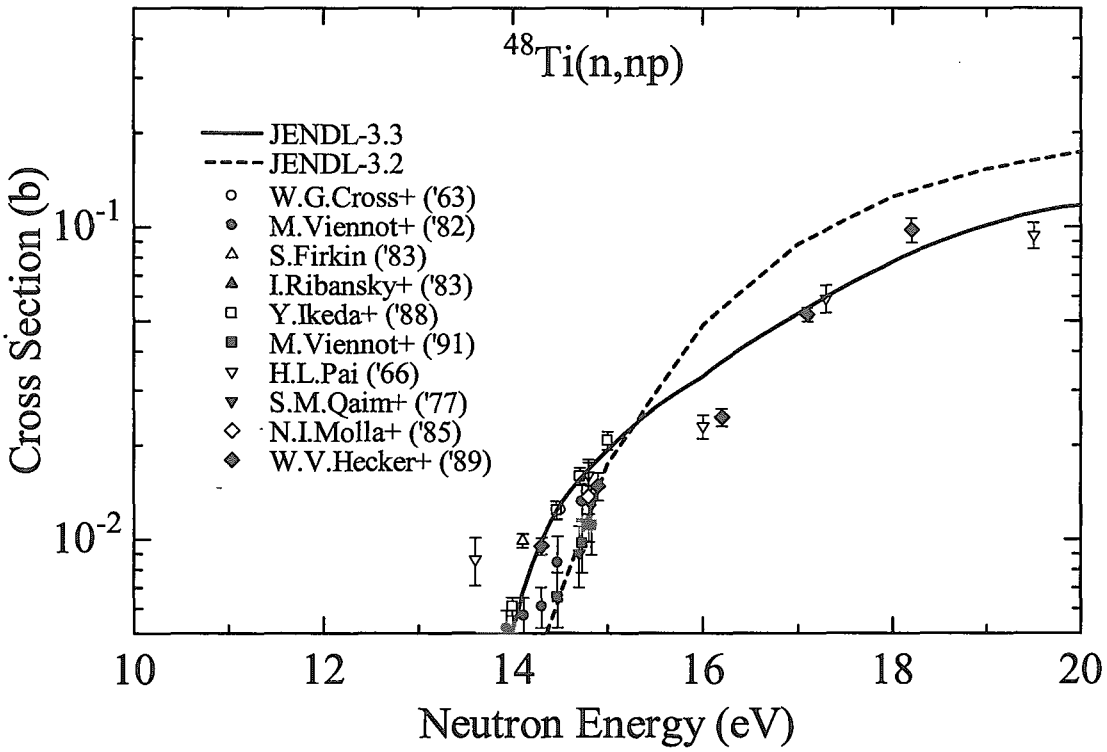


Fig. 7 $^{48}$Ti(n,np) cross section.

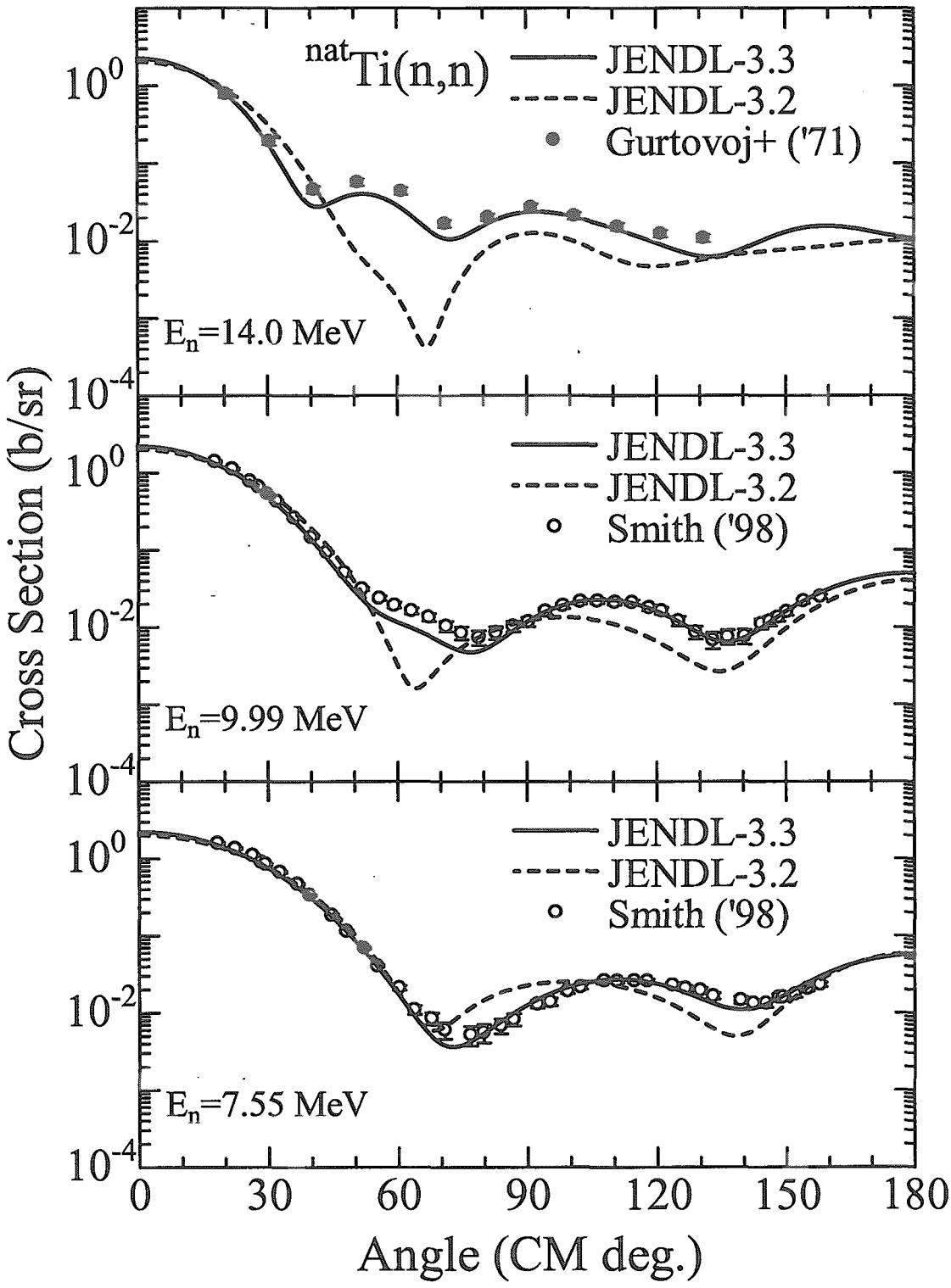


Fig. 8 Angular distributions of neutrons elastically scattered from elemental Ti.

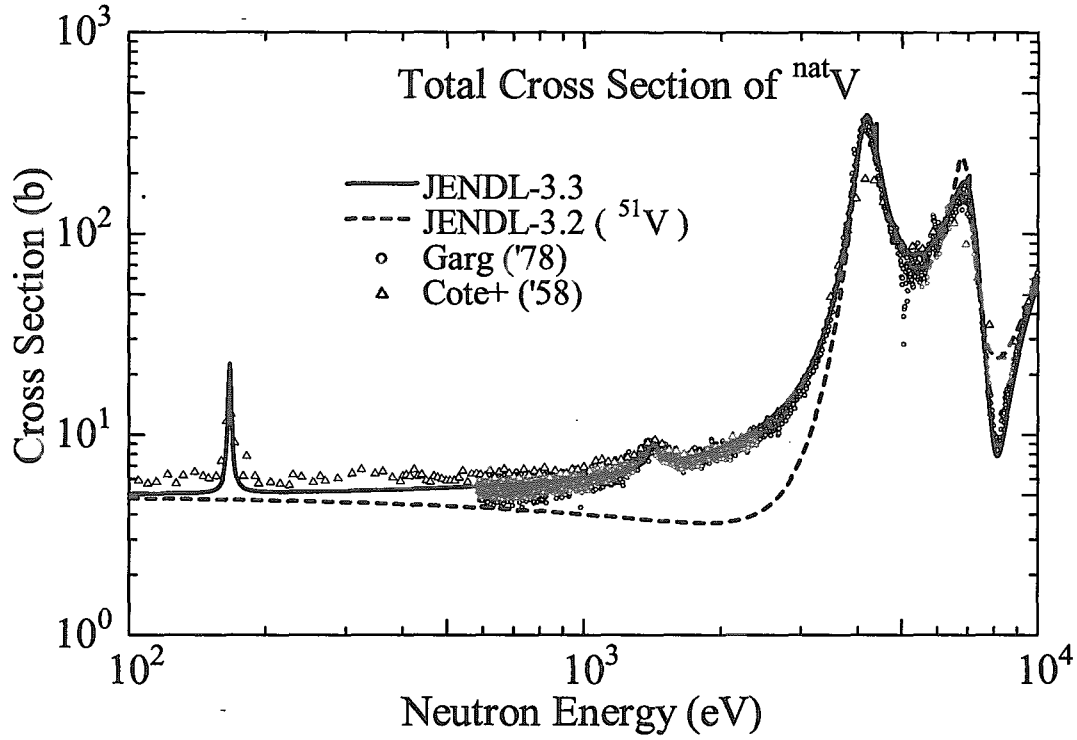


Fig. 9 Total cross section of elemental V in the resonance region.

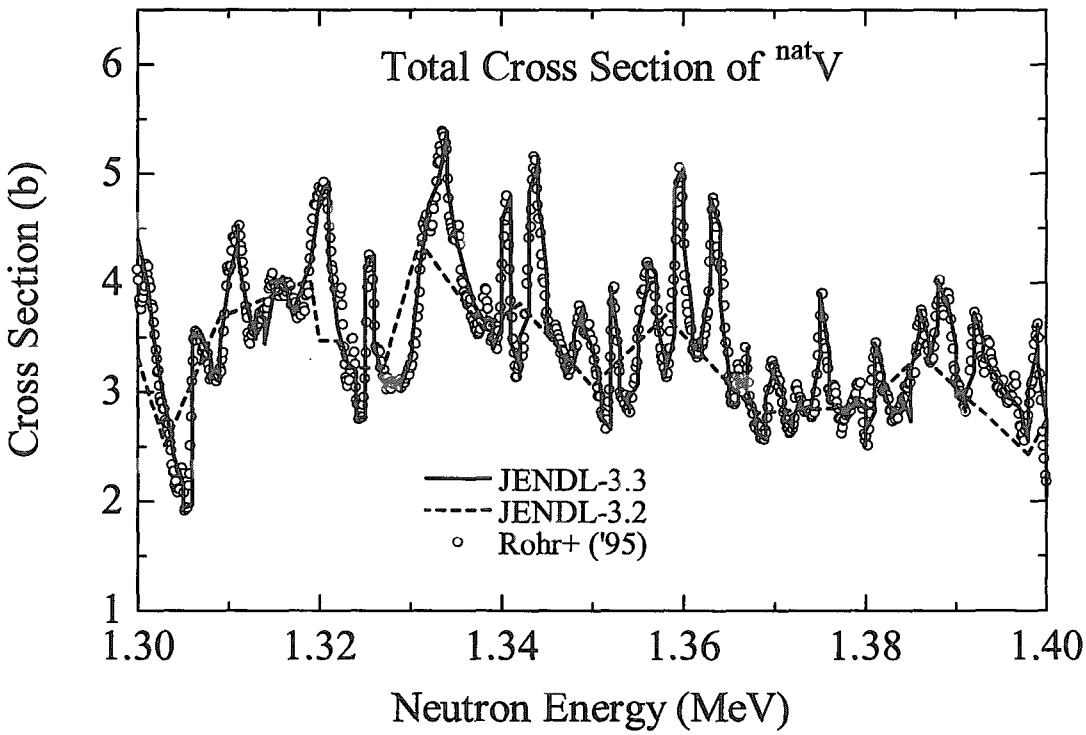


Fig. 10 Total cross section of elemental V between 1.3 and 1.4 MeV.

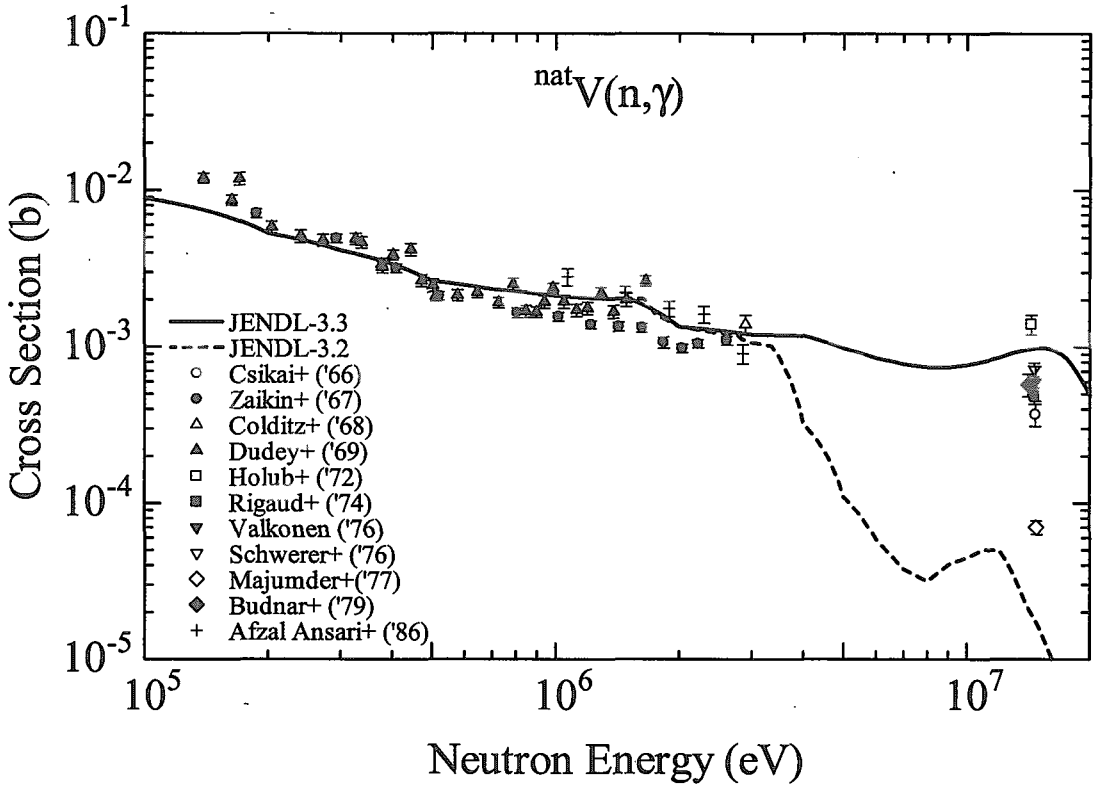


Fig. 11 Capture cross section of elemental V.

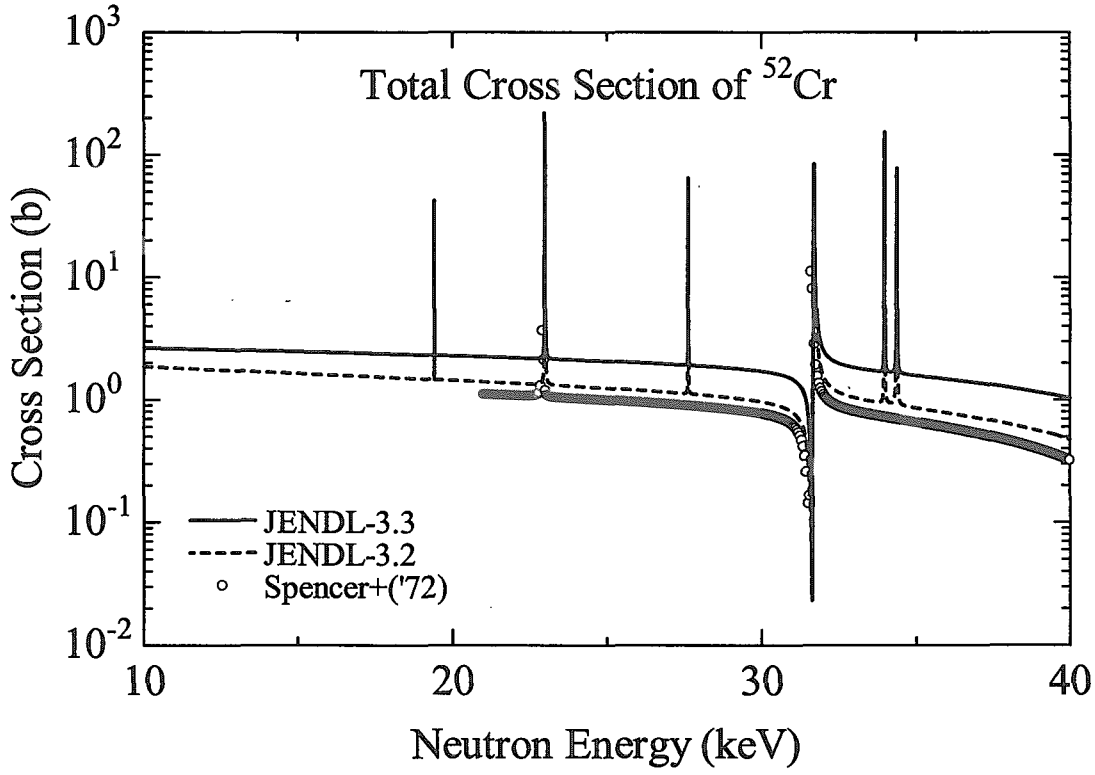


Fig. 12 Total cross section of $^{52}$Cr in the energy region from 10 to 40 keV.

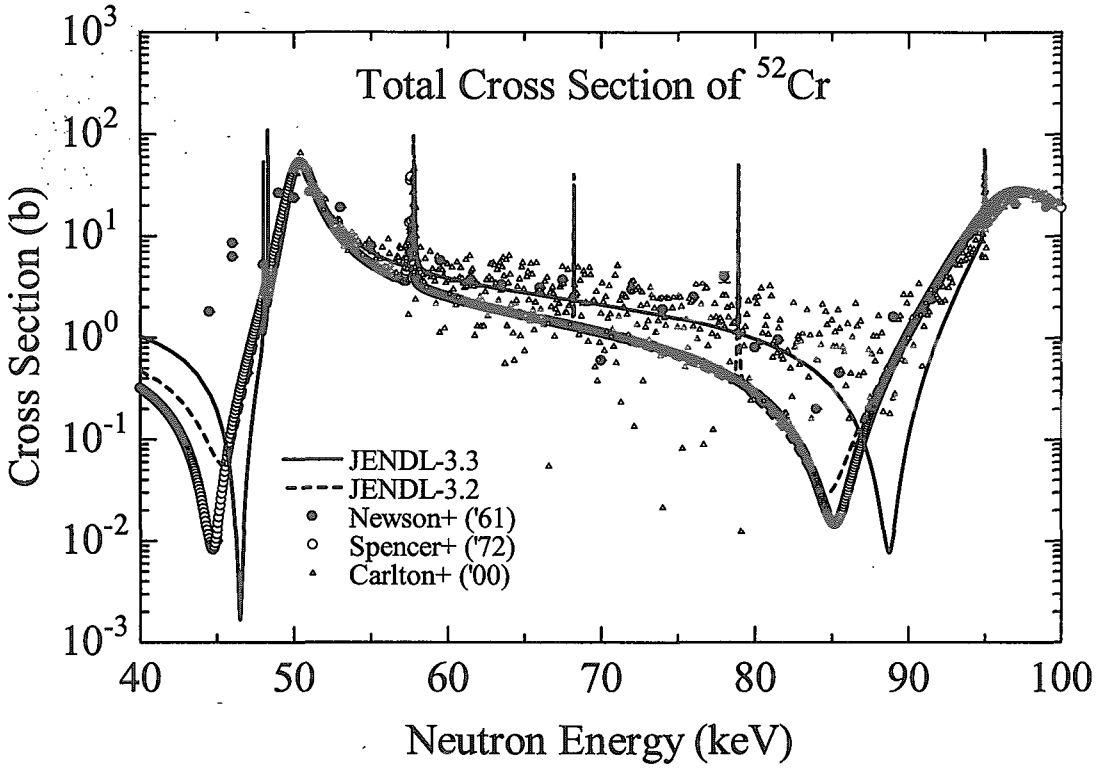


Fig. 13 Total cross section of $^{52}$Cr in the energy region from 40 to 100 keV.

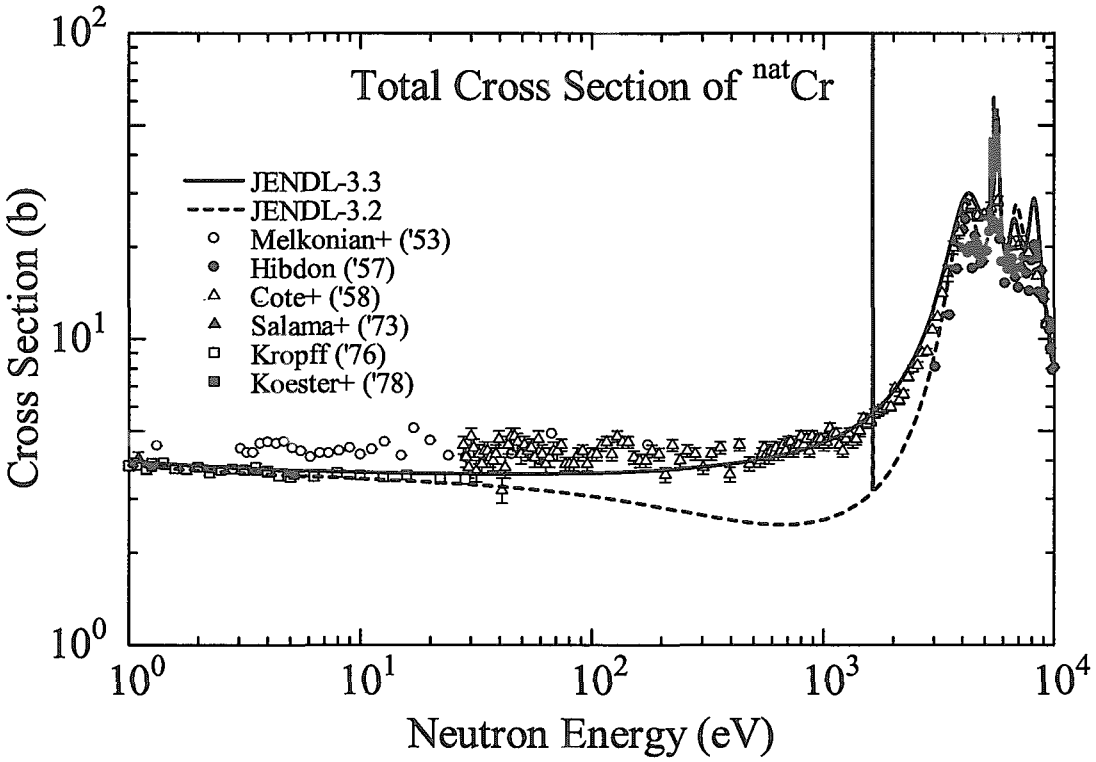


Fig. 14 Total cross section of elemental Cr in the energy region from 1 eV to 10 keV.

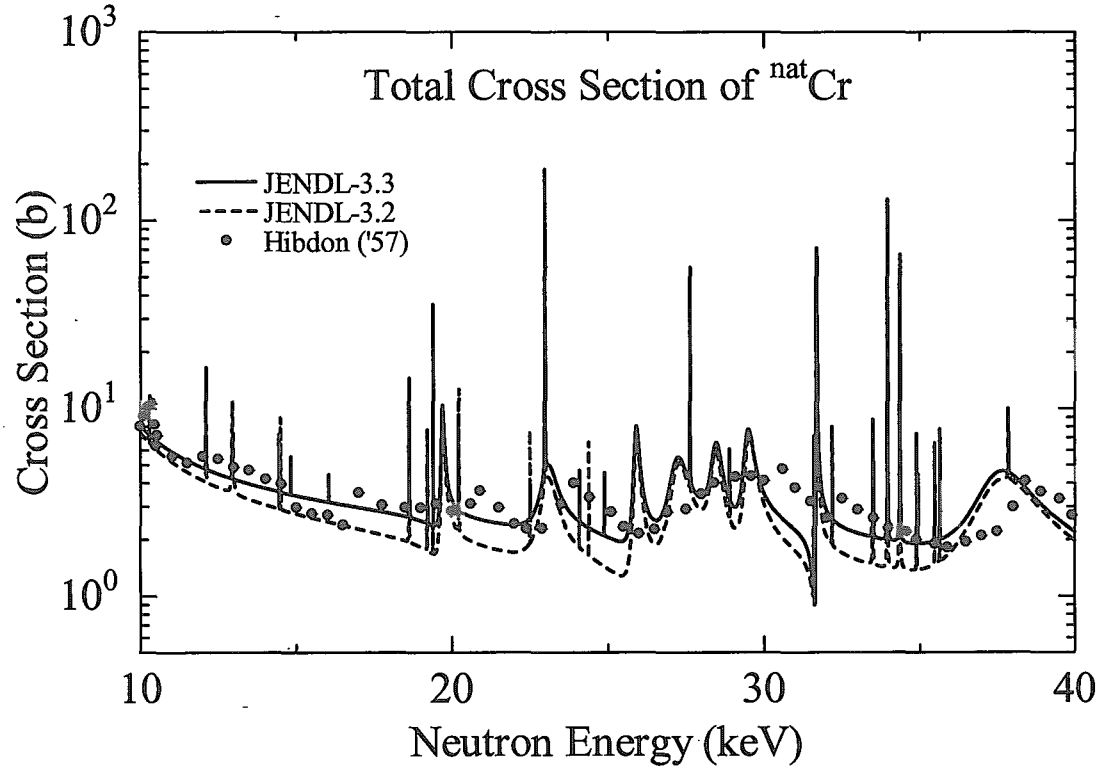


Fig. 15 Total cross section of elemental Cr in the energy region from 10 to 40 keV.

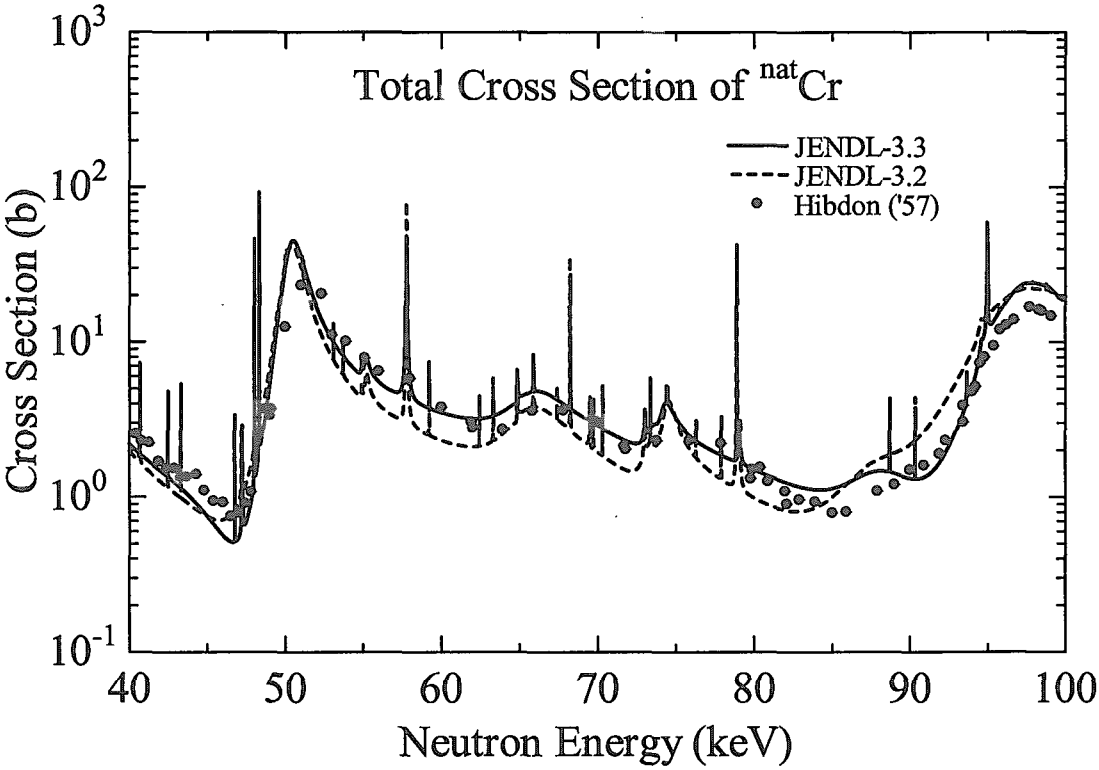


Fig. 16 Total cross section of elemental Cr in the energy region from 40 to 100 keV.

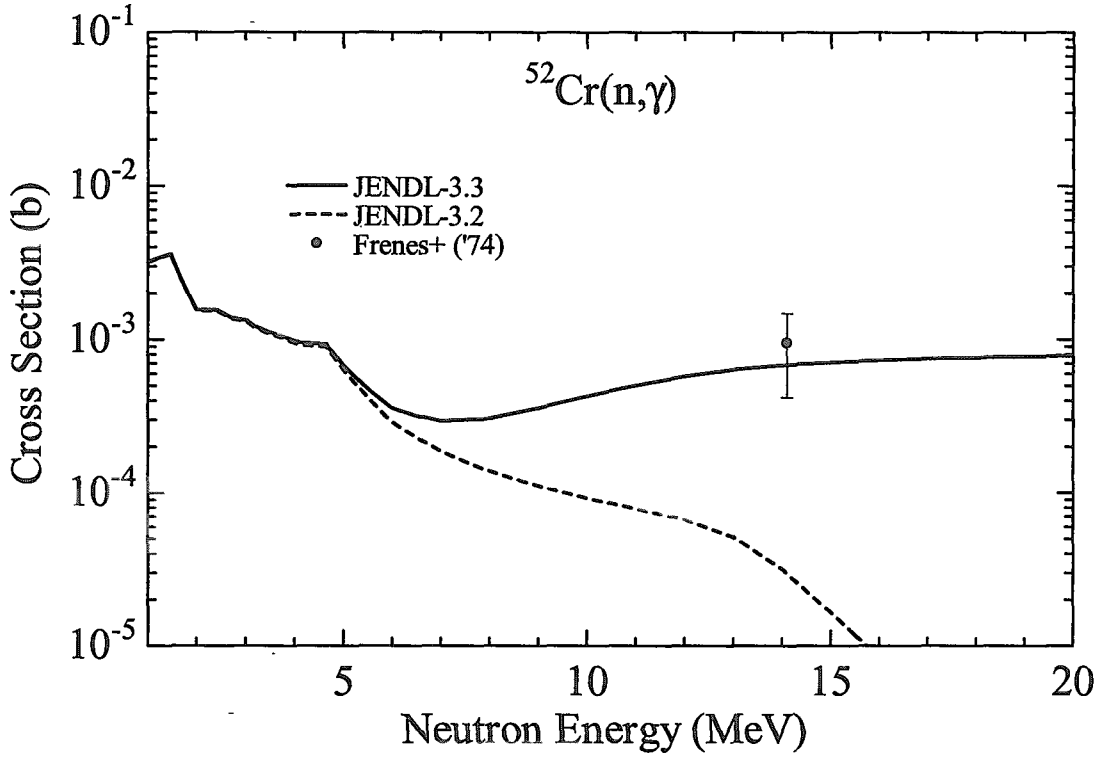


Fig. 17 Capture cross section of $^{52}$Cr.

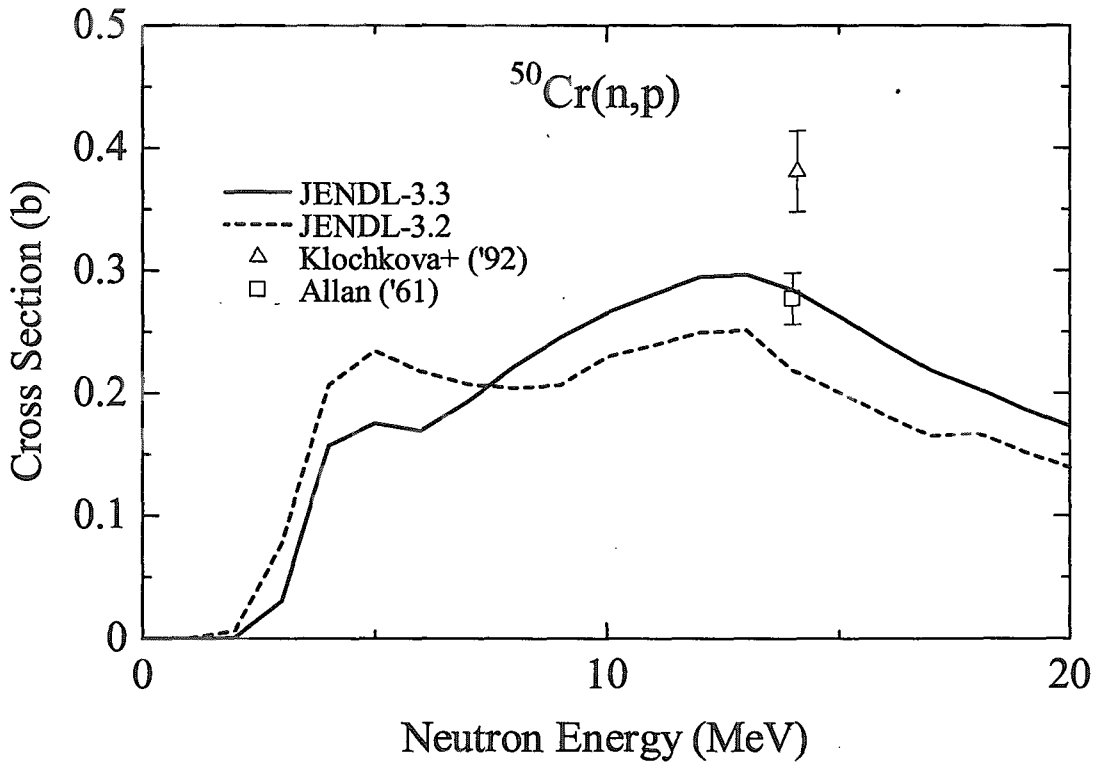


Fig. 18 $^{50}$Cr(n,p) cross section.

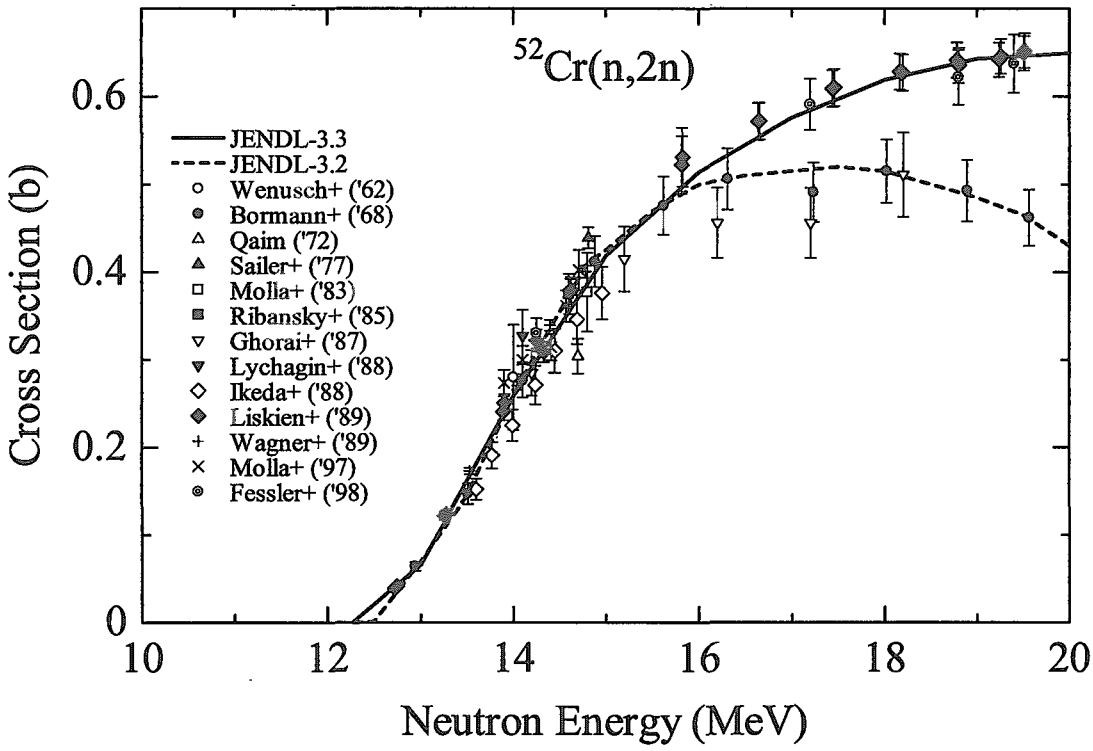


Fig. 19 $^{52}$Cr(n,2n) cross section.

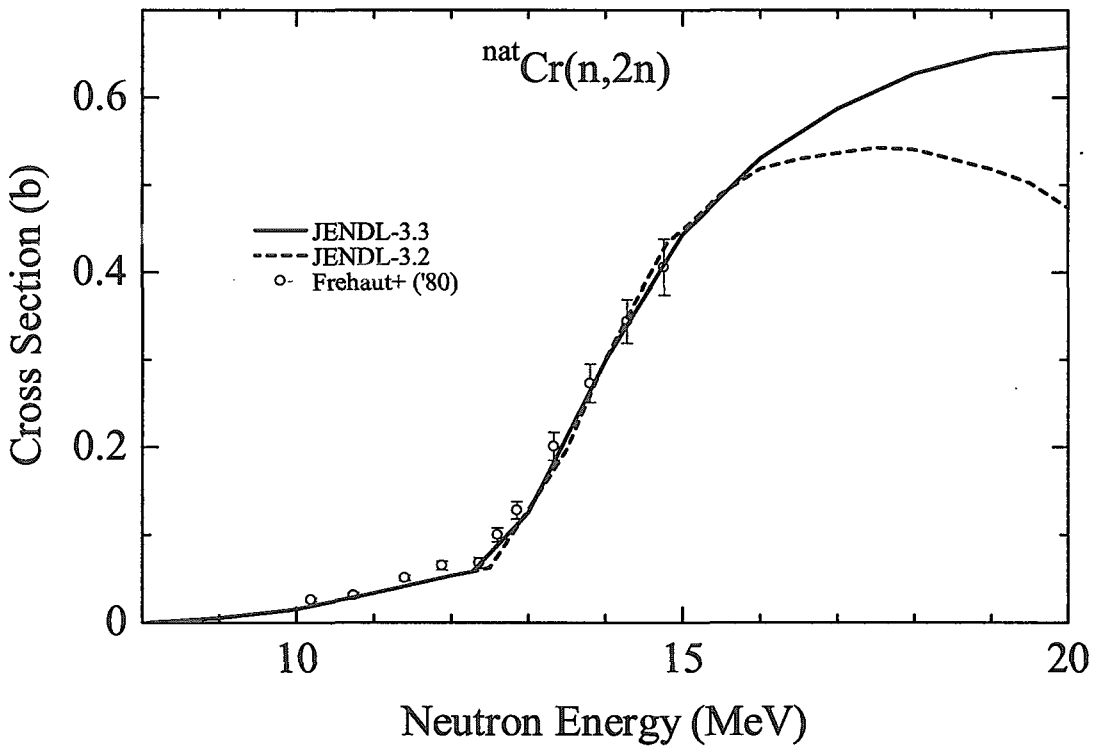


Fig. 20 $^{nat}$Cr(n,2n) cross section.

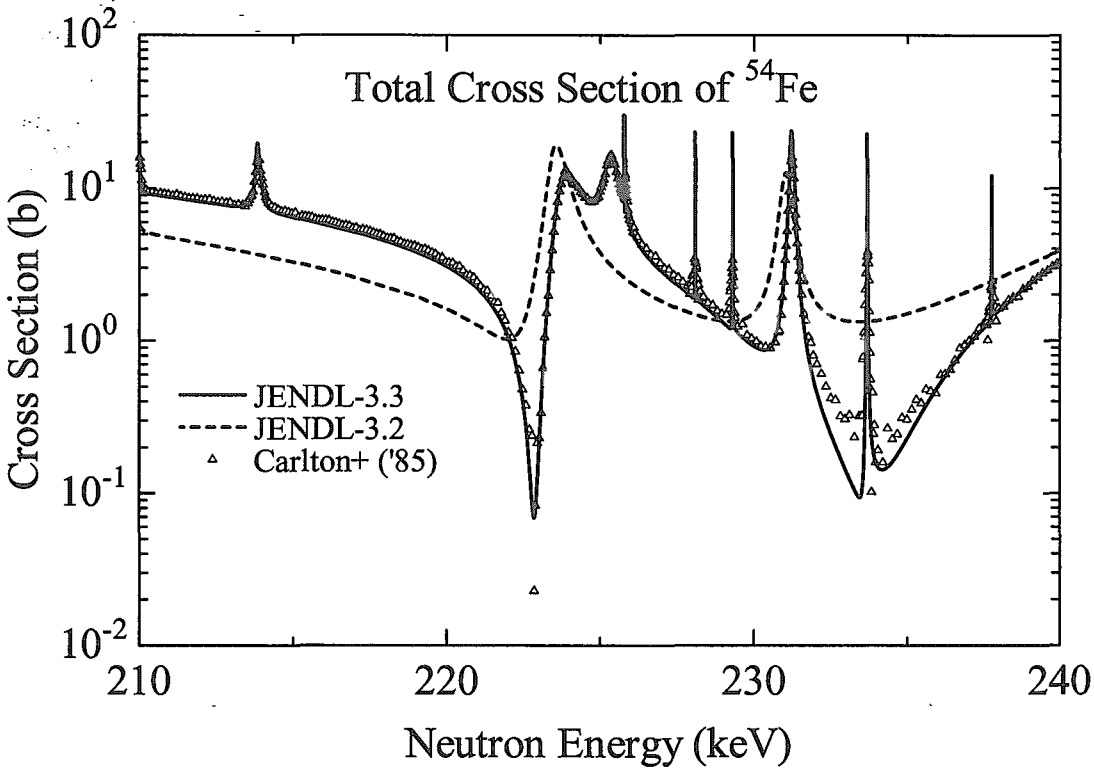


Fig. 21 Total cross section of $^{54}$Fe in the energy region from 210 to 240 keV.

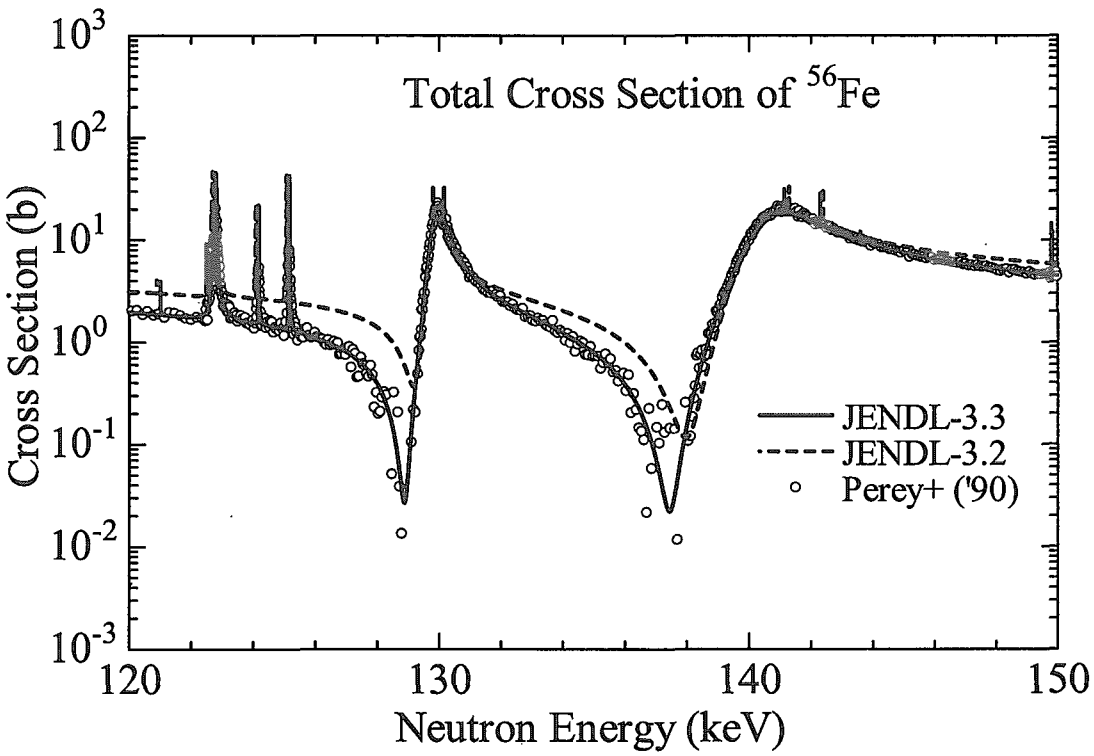


Fig 22 Total cross section of $^{56}$Fe in the energy region from 120 to 150 keV.

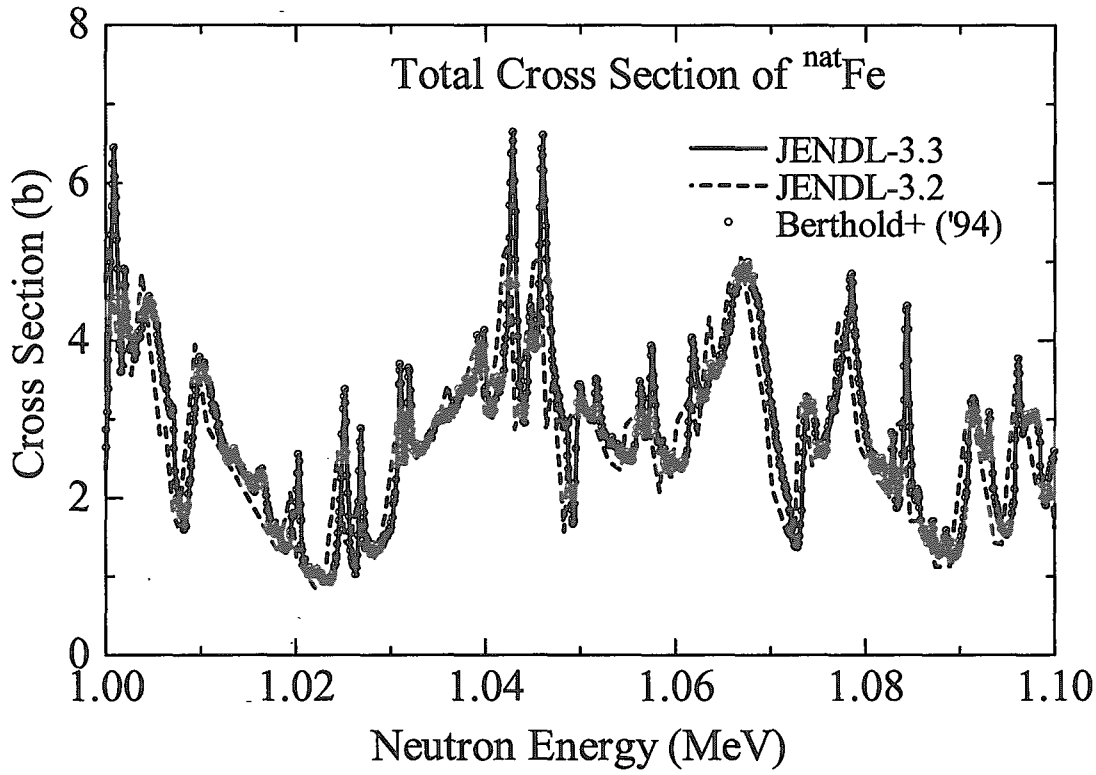


Fig. 23 Total cross section of $^{nat}$Fe in the energy region from 1.0 to 1.1 MeV.

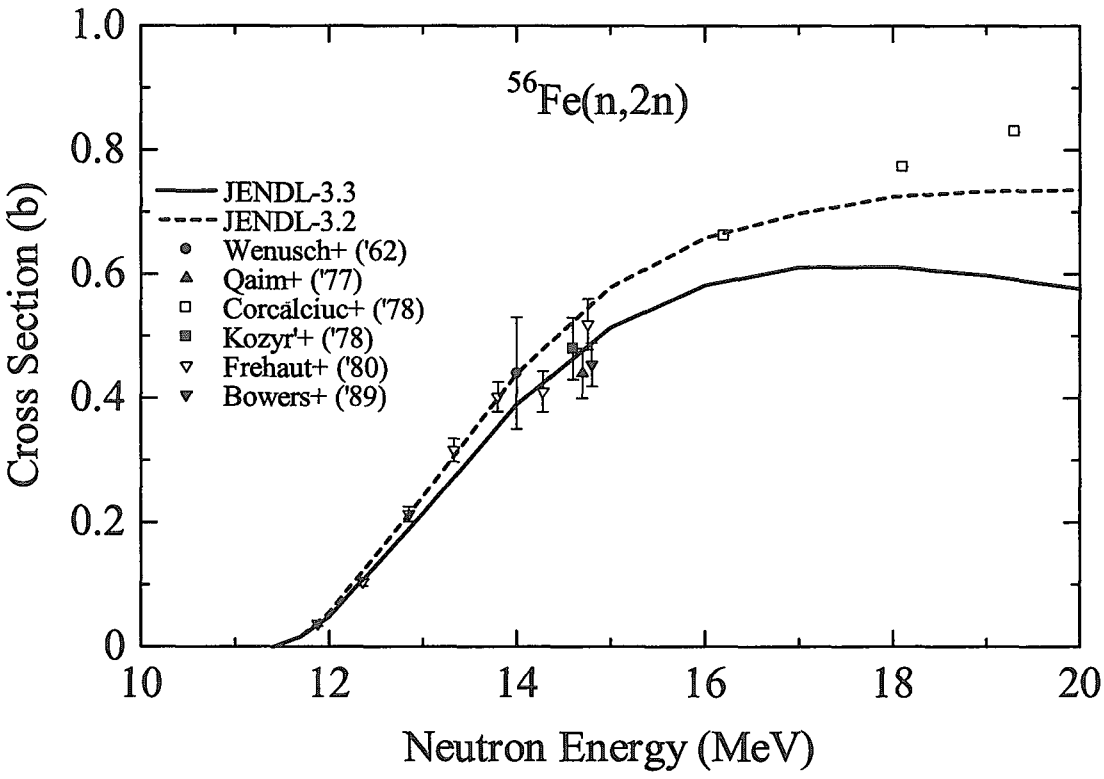


Fig. 24 $^{56}$Fe(n,2n) cross section.

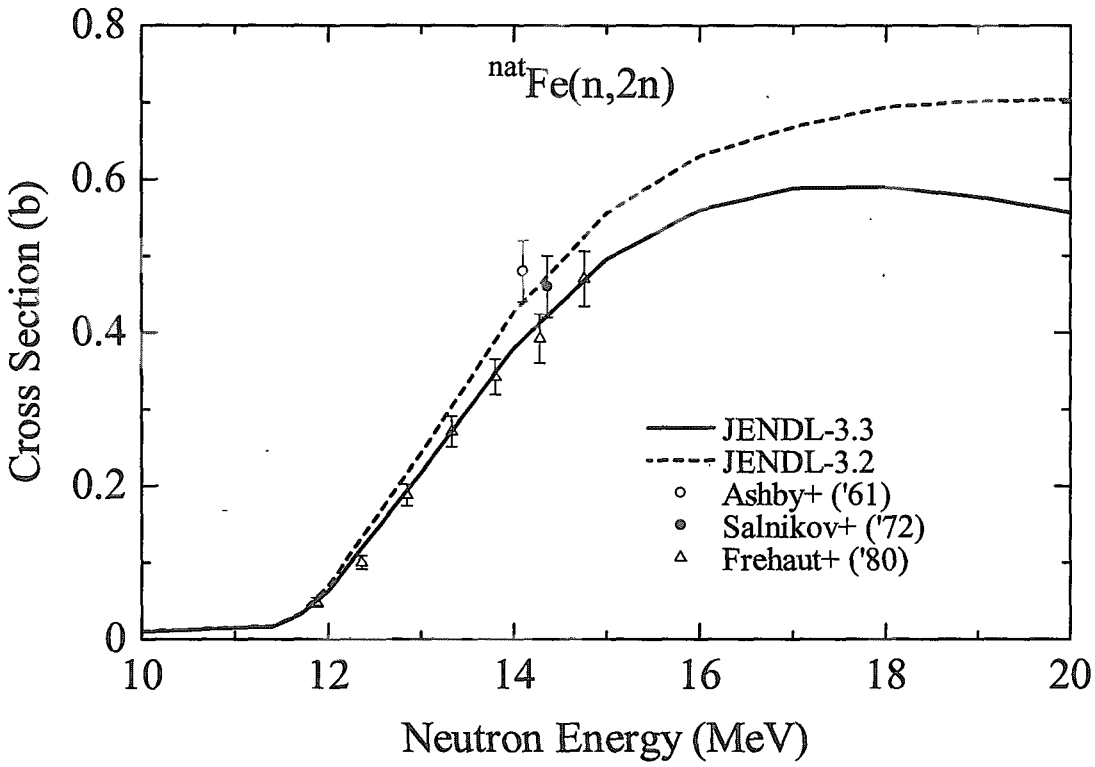


Fig. 25 $^{nat}$Fe(n,2n) cross section.

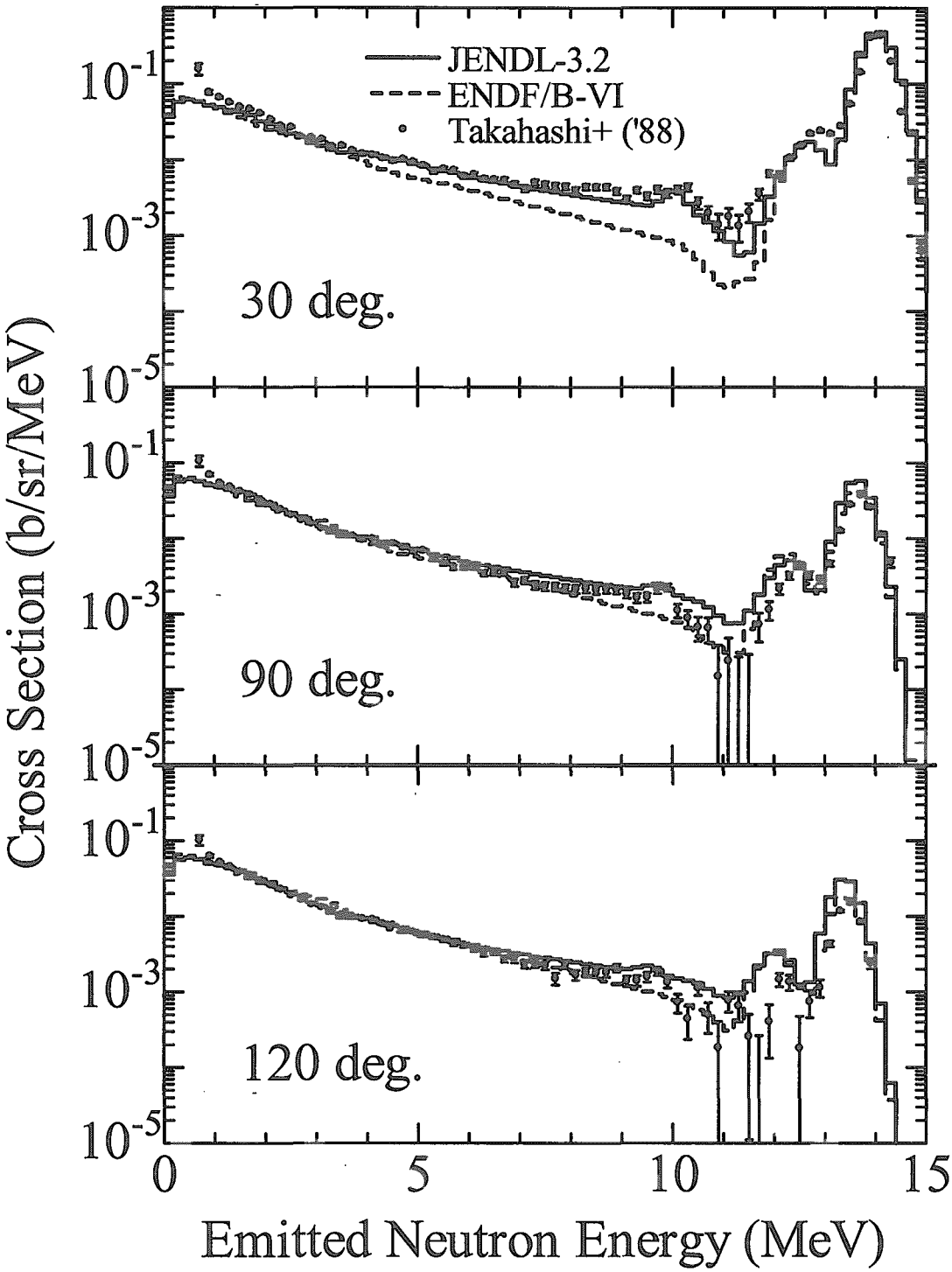


Fig. 26 Neutron emission spectra from $^{59}$Co at 14 MeV.

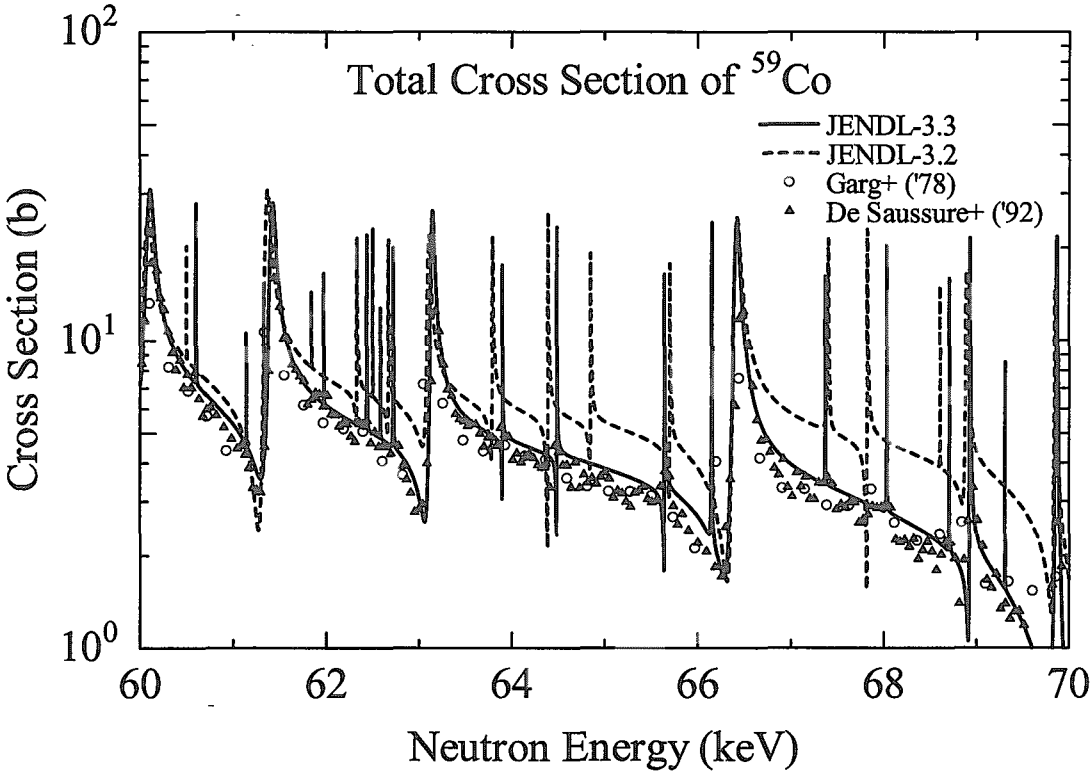


Fig. 27 Total cross section of $^{59}$Co in the energy region from 60 to 70 keV.

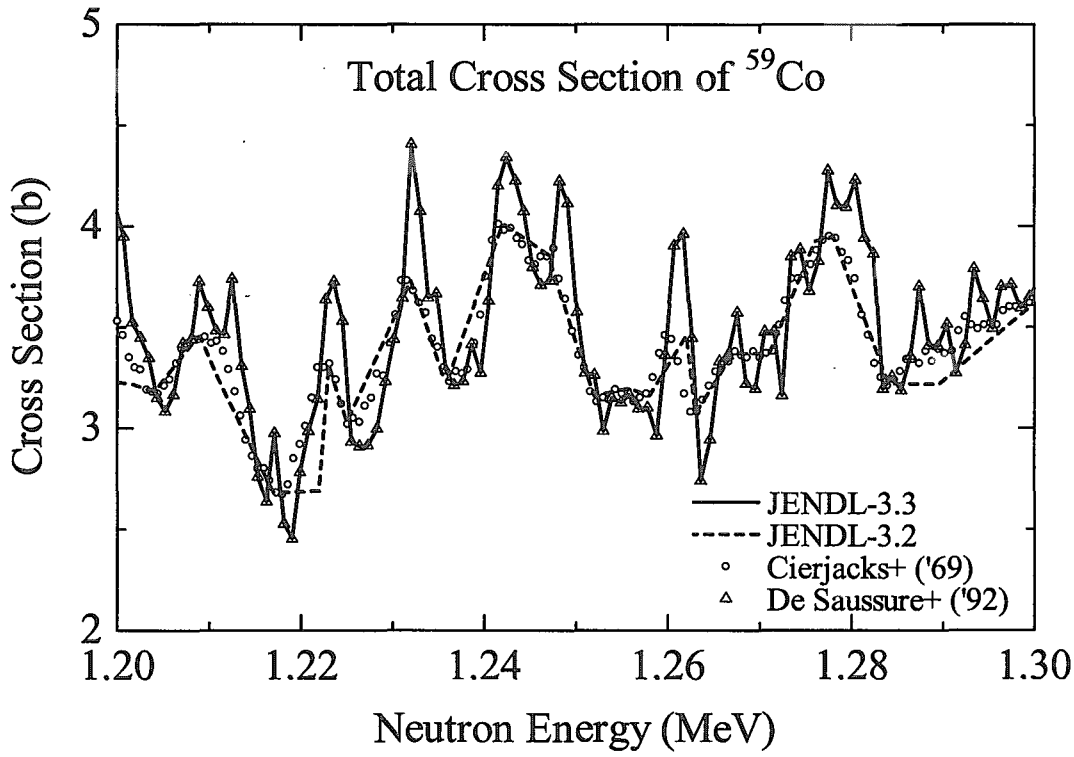


Fig. 28 Total cross section of $^{59}$Co in the energy region from 1.2 to 1.3 MeV.

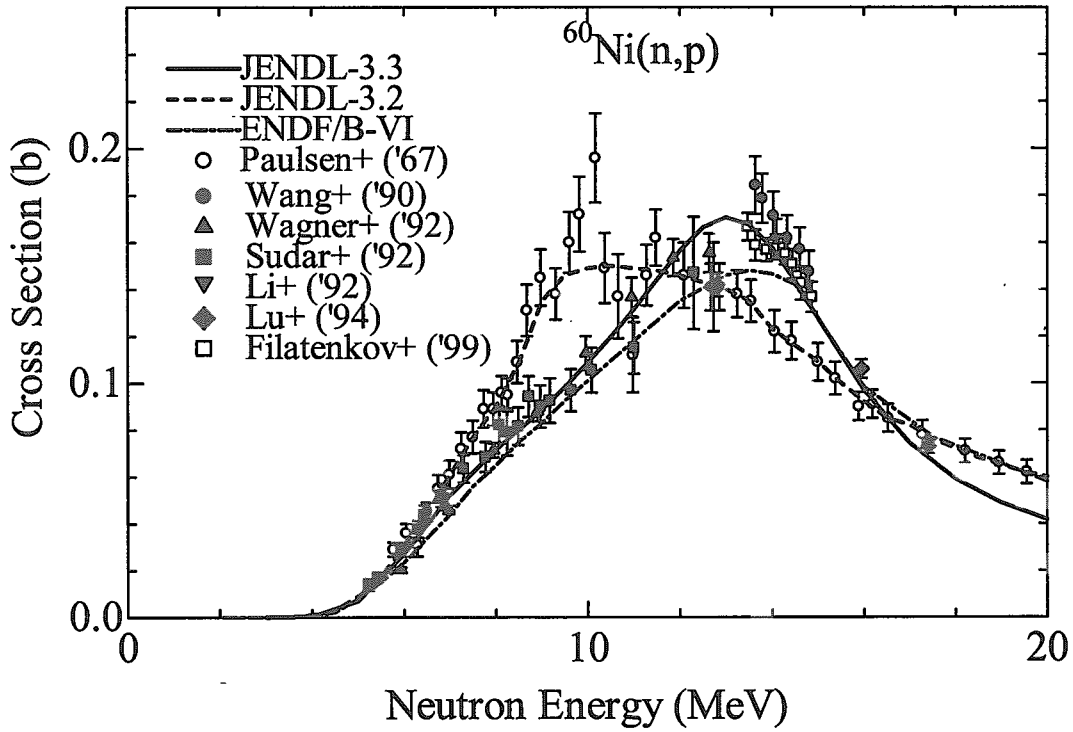


Fig. 29 $^{60}$Ni(n,p) cross section.

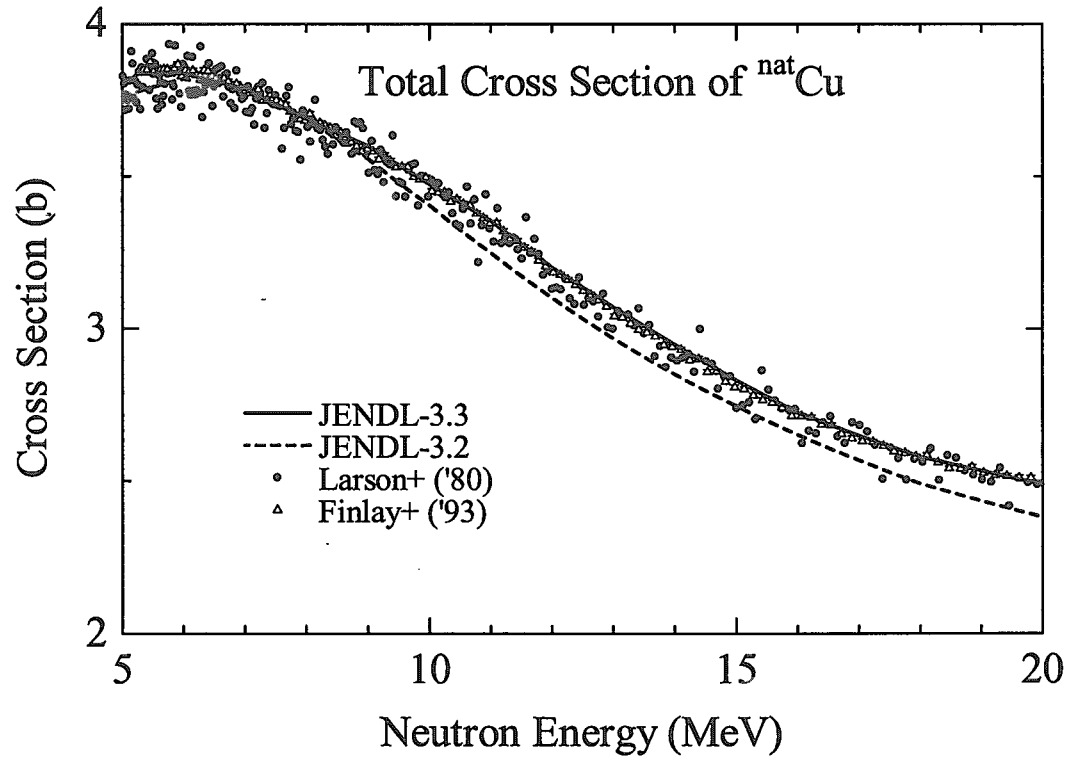


Fig. 30 Total cross section of $^{nat}$Cu.

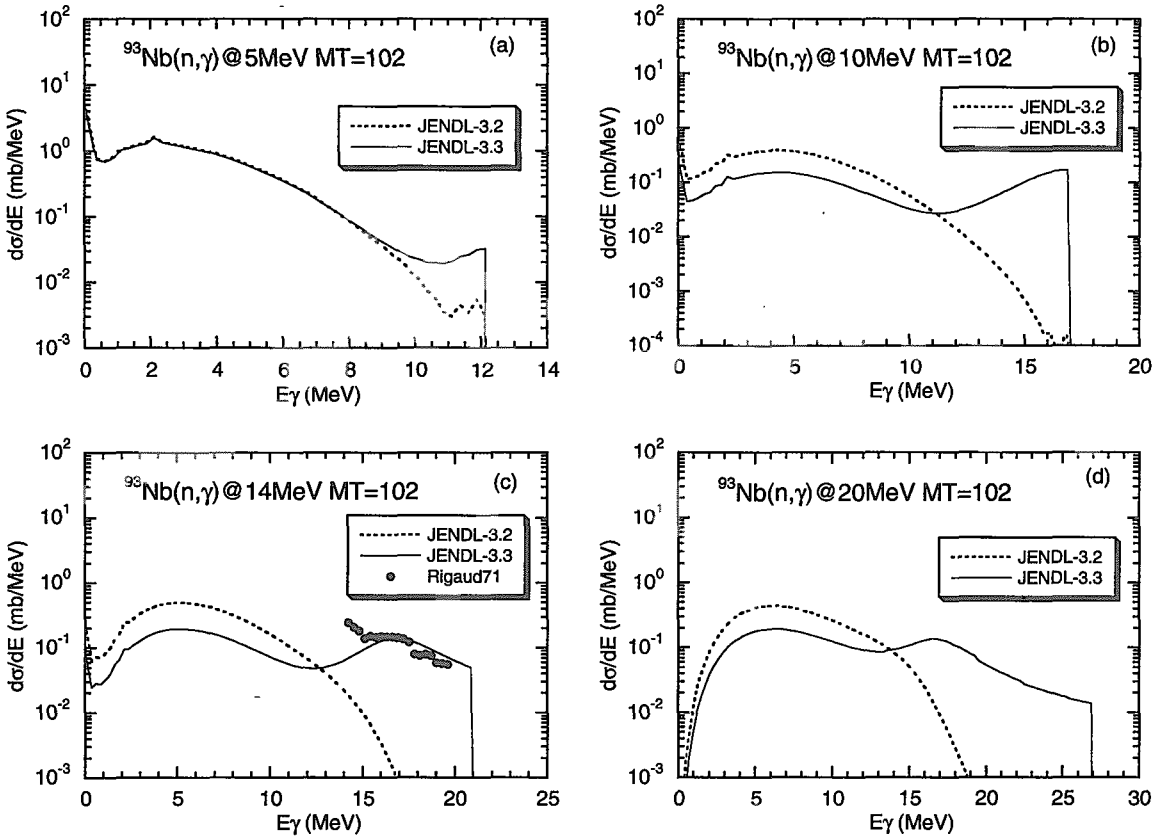


Fig. 31 Comparisons of the capture gamma-ray spectra between JENDL-3.3 and -3.2.

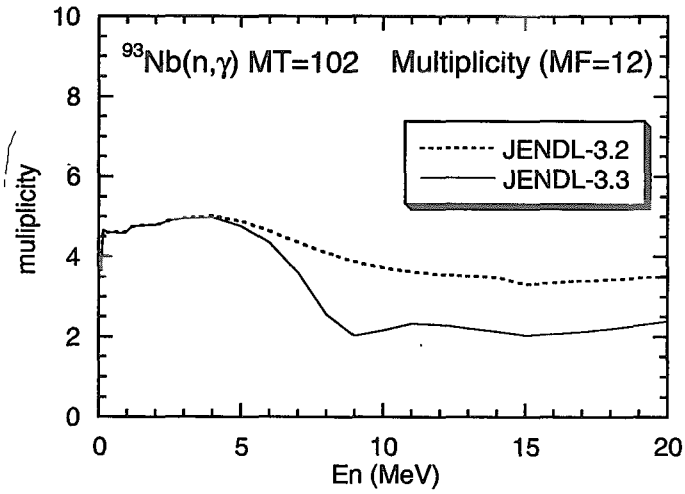


Fig. 32 Gamma-ray multiplicities given in JENDL-3.3 and -3.2.

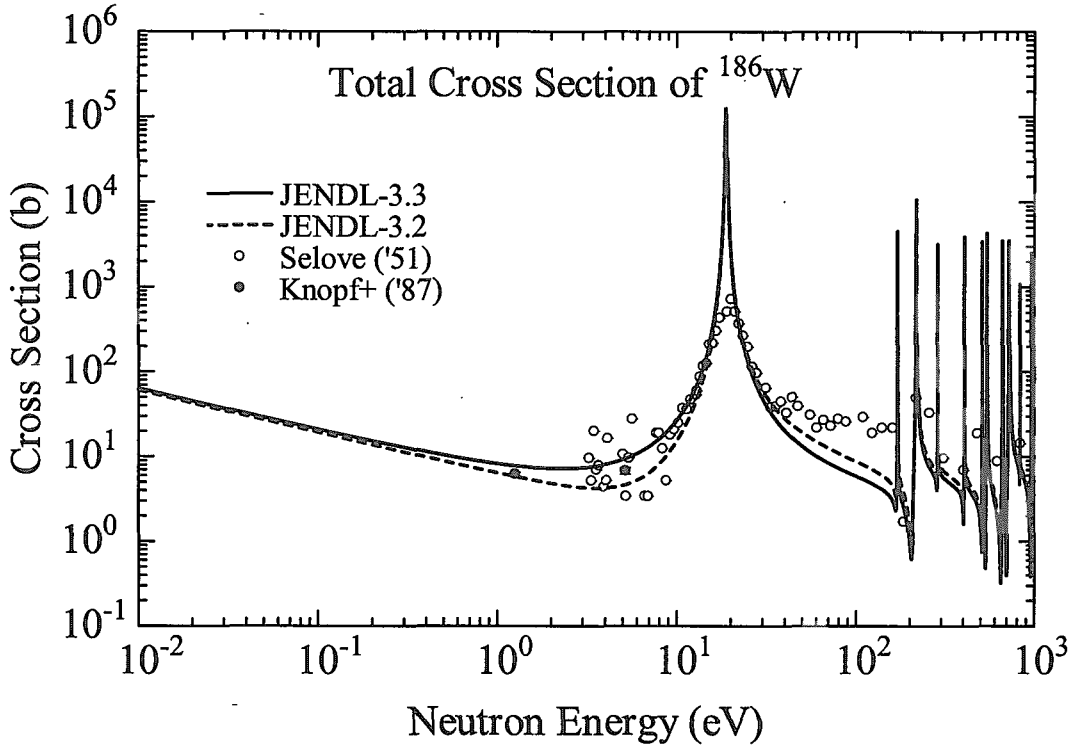


Fig. 33 Total cross section of $^{186}$W in the energy region from $10^{-2}$ eV to 1 keV.

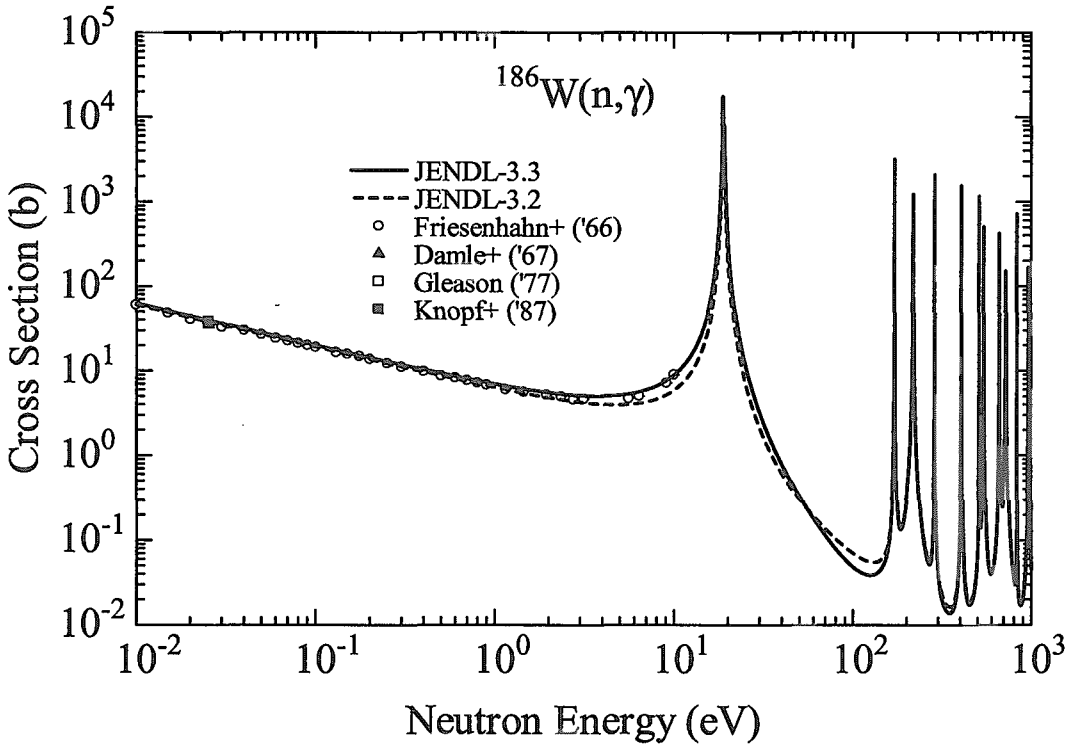


Fig. 34 Capture cross section of $^{186}$W in the energy region from $10^{-2}$ eV to 1 keV.

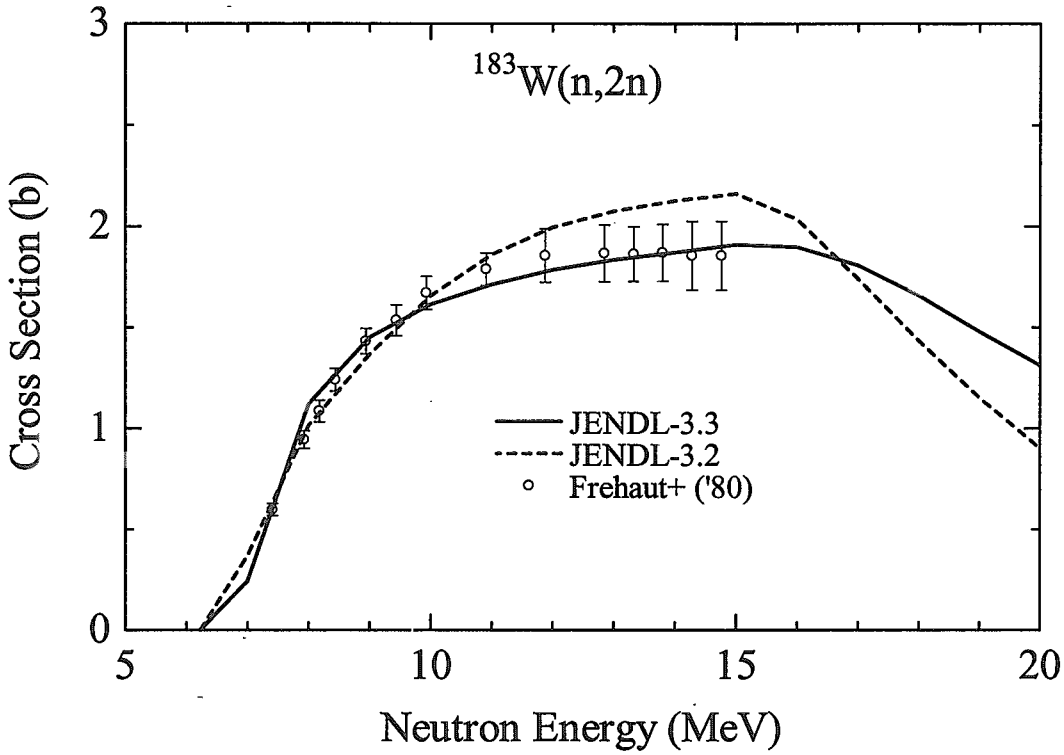


Fig. 35 $^{183}$W(n,2n) cross section.

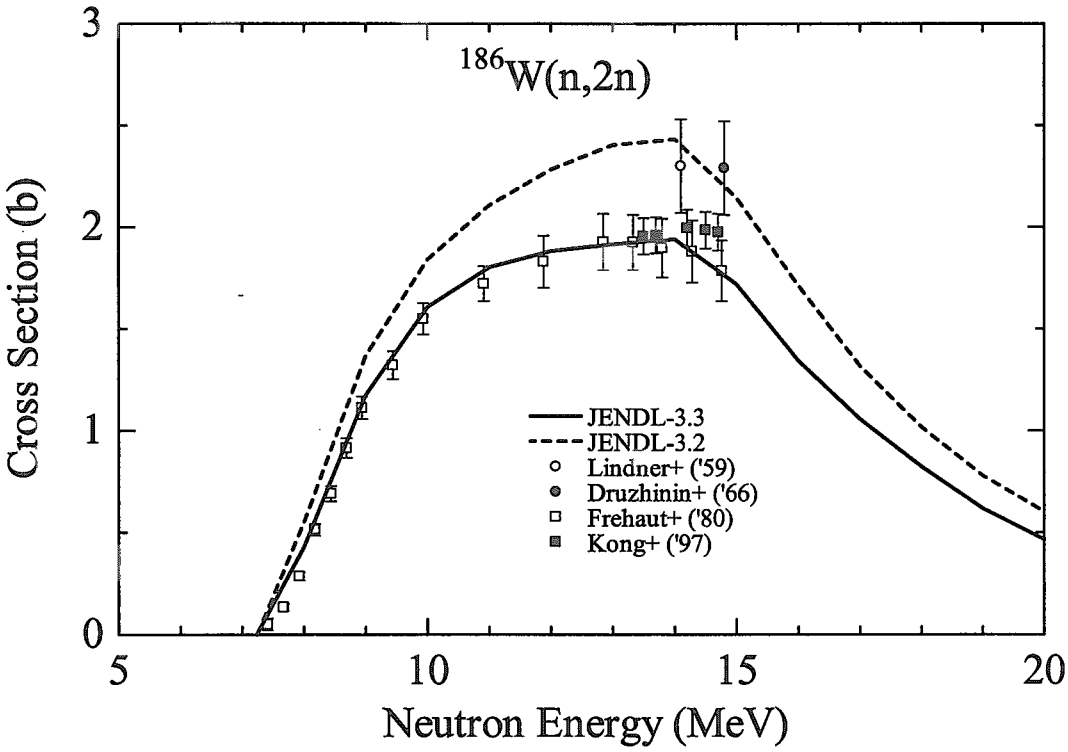


Fig. 36 $^{186}$W(n,2n) cross section.

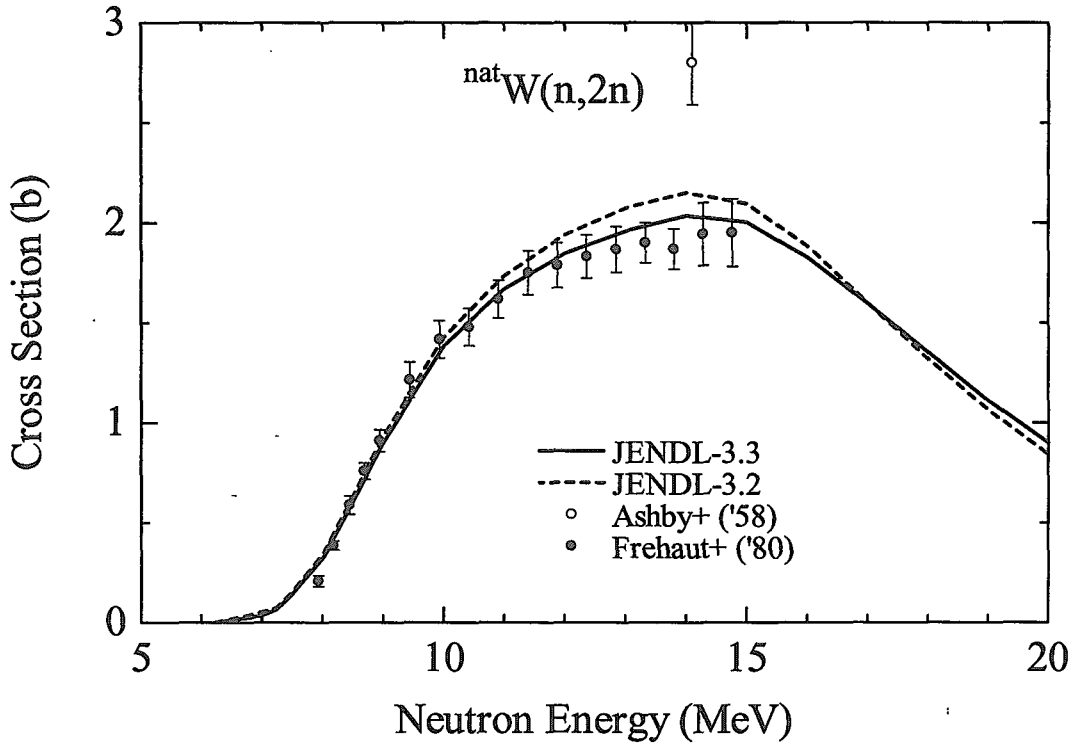


Fig. 37 $^{nat}$W(n,2n) cross section.

This is a blank page.

# 国際単位系 (SI) と換算表

表1　SI基本単位および補助単位

| 量 | 名称 | 記号 |
|---|---|---|
| 長さ | メートル | m |
| 質量 | キログラム | kg |
| 時間 | 秒 | s |
| 電流 | アンペア | A |
| 熱力学温度 | ケルビン | K |
| 物質量 | モル | mol |
| 光度 | カンデラ | cd |
| 平面角 | ラジアン | rad |
| 立体角 | ステラジアン | sr |

表2　SIと併用される単位

| 名称 | 記号 |
|---|---|
| 分，時，日 | min，h，d |
| 度，分，秒 | °，′，″ |
| リットル | l，L |
| トン | t |
| 電子ボルト | eV |
| 原子質量単位 | u |

1 eV=1.60218×$10^{-19}$J

1 u=1.66054×$10^{-27}$kg

表3　固有の名称をもつSI組立単位

| 量 | 名称 | 記号 | 他のSI単位による表現 |
|---|---|---|---|
| 周波数 | ヘルツ | Hz | $s^{-1}$ |
| 力 | ニュートン | N | m·kg/$s^2$ |
| 圧力，応力 | パスカル | Pa | N/$m^2$ |
| エネルギー，仕事，熱量 | ジュール | J | N·m |
| 工率，放射束 | ワット | W | J/s |
| 電気量，電荷 | クーロン | C | A·s |
| 電位，電圧，起電力 | ボルト | V | W/A |
| 静電容量 | ファラド | F | C/V |
| 電気抵抗 | オーム | Ω | V/A |
| コンダクタンス | ジーメンス | S | A/V |
| 磁束 | ウェーバ | Wb | V·s |
| 磁束密度 | テスラ | T | Wb/$m^2$ |
| インダクタンス | ヘンリー | H | Wb/A |
| セルシウス温度 | セルシウス度 | ℃ | |
| 光束 | ルーメン | lm | cd·sr |
| 照度 | ルクス | lx | lm/$m^2$ |
| 放射能 | ベクレル | Bq | $s^{-1}$ |
| 吸収線量 | グレイ | Gy | J/kg |
| 線量当量 | シーベルト | Sv | J/kg |

表4　SIと共に暫定的に維持される単位

| 名称 | 記号 |
|---|---|
| オングストローム | Å |
| バーン | b |
| バール | bar |
| ガル | Gal |
| キュリー | Ci |
| レントゲン | R |
| ラド | rad |
| レム | rem |

1 Å=0.1 nm=$10^{-10}$m

1 b=100 $fm^2$=$10^{-28}$ $m^2$

1 bar=0.1 MPa=$10^5$Pa

1 Gal=1 cm/$s^2$=$10^{-2}$m/$s^2$

1 Ci=3.7×$10^{10}$Bq

1 R=2.58×$10^{-4}$C/kg

1 rad=1 cGy=$10^{-2}$Gy

1 rem=1 cSv=$10^{-2}$Sv

表5　SI接頭語

| 倍数 | 接頭語 | 記号 |
|---|---|---|
| $10^{18}$ | エクサ | E |
| $10^{15}$ | ペタ | P |
| $10^{12}$ | テラ | T |
| $10^{9}$ | ギガ | G |
| $10^{6}$ | メガ | M |
| $10^{3}$ | キロ | k |
| $10^{2}$ | ヘクト | h |
| $10^{1}$ | デカ | da |
| $10^{-1}$ | デシ | d |
| $10^{-2}$ | センチ | c |
| $10^{-3}$ | ミリ | m |
| $10^{-6}$ | マイクロ | μ |
| $10^{-9}$ | ナノ | n |
| $10^{-12}$ | ピコ | p |
| $10^{-15}$ | フェムト | f |
| $10^{-18}$ | アト | a |

（注）

1. 表1－5は「国際単位系」第5版，国際度量衡局 1985年刊行による。ただし，1 eVおよび1 uの値はCODATAの1986年推奨値によった。
2. 表4には海里，ノット，アール，ヘクタールも含まれているが日常の単位なのでここでは省略した。
3. barは，JISでは流体の圧力を表わす場合に限り表2のカテゴリーに分類されている。
4. EC閣僚理事会指令ではbar，barnおよび「血圧の単位」mmHgを表2のカテゴリーに入れている。

換　算　表

| 力 | N(=$10^5$dyn) | kgf | lbf |
|---|---|---|---|
| | 1 | 0.101972 | 0.224809 |
| | 9.80665 | 1 | 2.20462 |
| | 4.44822 | 0.453592 | 1 |

粘度　1 Pa·s(N·s/$m^2$)=10 P(ポアズ)(g/(cm·s))

動粘度　1 $m^2$/s=$10^4$St(ストークス)($cm^2$/s)

| 圧力 | MPa(=10 bar) | kgf/$cm^2$ | atm | mmHg(Torr) | lbf/$in^2$(psi) |
|---|---|---|---|---|---|
| | 1 | 10.1972 | 9.86923 | 7.50062×$10^3$ | 145.038 |
| | 0.0980665 | 1 | 0.967841 | 735.559 | 14.2233 |
| | 0.101325 | 1.03323 | 1 | 760 | 14.6959 |
| | 1.33322×$10^{-4}$ | 1.35951×$10^{-3}$ | 1.31579×$10^{-3}$ | 1 | 1.93368×$10^{-2}$ |
| | 6.89476×$10^{-3}$ | 7.03070×$10^{-2}$ | 6.80460×$10^{-2}$ | 51.7149 | 1 |

| エネルギー・仕事・熱量 | J(=$10^7$erg) | kgf·m | kW·h | cal(計量法) | Btu | ft·lbf | eV |
|---|---|---|---|---|---|---|---|
| | 1 | 0.101972 | 2.77778×$10^{-7}$ | 0.238889 | 9.47813×$10^{-4}$ | 0.737562 | 6.24150×$10^{18}$ |
| | 9.80665 | 1 | 2.72407×$10^{-6}$ | 2.34270 | 9.29487×$10^{-3}$ | 7.23301 | 6.12082×$10^{19}$ |
| | 3.6×$10^6$ | 3.67098×$10^5$ | 1 | 8.59999×$10^5$ | 3412.13 | 2.65522×$10^6$ | 2.24694×$10^{25}$ |
| | 4.18605 | 0.426858 | 1.16279×$10^{-6}$ | 1 | 3.96759×$10^{-3}$ | 3.08747 | 2.61272×$10^{19}$ |
| | 1055.06 | 107.586 | 2.93072×$10^{-4}$ | 252.042 | 1 | 778.172 | 6.58515×$10^{21}$ |
| | 1.35582 | 0.138255 | 3.76616×$10^{-7}$ | 0.323890 | 1.28506×$10^{-3}$ | 1 | 8.46233×$10^{18}$ |
| | 1.60218×$10^{-19}$ | 1.63377×$10^{-20}$ | 4.45050×$10^{-26}$ | 3.82743×$10^{-20}$ | 1.51857×$10^{-22}$ | 1.18171×$10^{-19}$ | 1 |

1 cal = 4.18605 J（計量法）

= 4.184 J　（熱化学）

= 4.1855 J（15 °C）

= 4.1868 J（国際蒸気表）

仕事率　1 PS（仏馬力）

= 75 kgf·m/s

= 735.499 W

| 放射能 | Bq | Ci |
|---|---|---|
| | 1 | 2.70270×$10^{-11}$ |
| | 3.7×$10^{10}$ | 1 |

| 吸収線量 | Gy | rad |
|---|---|---|
| | 1 | 100 |
| | 0.01 | 1 |

| 照射線量 | C/kg | R |
|---|---|---|
| | 1 | 3876 |
| | 2.58×$10^{-4}$ | 1 |

| 線量当量 | Sv | rem |
|---|---|---|
| | 1 | 100 |
| | 0.01 | 1 |

（86年12月26日現在）

Evaluations of Medium-heavy Nuclide Data for JENDL-3.3